Knockout of the BK β2 subunit abolishes inactivation of BK currents in mouse adrenal chromaffin cells and results in slow-wave burst activity

Pedro L. Martinez-Espinosa, Chengtao Yang, Vivian Gonzalez-Perez, Xiao-Ming Xia, and Christopher J. Lingle

Department of Anesthesiology, Washington University School of Medicine in St. Louis, St. Louis, MO 63110

Rat and mouse adrenal medullary chromaffin cells (CCs) express an inactivating BK current. This inactivation is thought to arise from the assembly of up to four β2 auxiliary subunits (encoded by the *kcnmb2* gene) with a tetramer of pore-forming Slo1 α subunits. Although the physiological consequences of inactivation remain unclear, differences in depolarization-evoked firing among CCs have been proposed to arise from the ability of β2 subunits to shift the range of BK channel activation. To investigate the role of BK channels containing β2 subunits, we generated mice in which the gene encoding β2 was deleted (β2 knockout [KO]). Comparison of proteins from wild-type (WT) and β2 KO mice allowed unambiguous demonstration of the presence of β2 subunit in various tissues and its coassembly with the Slo1 α subunit. We compared current properties and cell firing properties of WT and β2 KO CCs in slices and found that β2 KO abolished inactivation, slowed action potential (AP) repolarization, and, during constant current injection, decreased AP firing. These results support the idea that the β2-mediated shift of the BK channel activation range affects repetitive firing and AP properties. Unexpectedly, CCs from β2 KO mice show an increased tendency toward spontaneous burst firing, suggesting that the particular properties of BK channels in the absence of β2 subunits may predispose to burst firing.

INTRODUCTION

Despite the widespread expression of Ca^{2+} and voltage-activated BK-type large conductance K^+ channels among different tissues, the specific physiological roles of such channels remain imperfectly understood in many tissues. Because activation of BK channels is promoted by both membrane depolarization and elevations of cytosolic Ca^{2+}, rapid activation of BK channels in many excitable cells may reduce peak action potential (AP) amplitude (Van Goor et al., 2001), may contribute to rapid repolarization after the AP peak (Solaro et al., 1995; Shao et al., 1999; Vandael et al., 2010), and then may contribute to relatively brief afterhyperpolarizations (AHPs) following APs (Sausbier et al., 2004; Contreras et al., 2013; Hoshi et al., 2013). However, often because of the simultaneous presence of other voltage-activated K^+ currents, specific inhibition of BK channels may have only modest effects on either AP durations or AHPs. Furthermore, the extent to which the molecular composition, i.e., the pore-forming α subunit splice variants, associated auxiliary subunits, or other soluble factors, of a given set of BK channels in a cell is suited to play a specific physiological role is little understood. Thus, despite the unambiguous presence of BK channels in a wide range of cells, hypotheses about physiological roles are often based on conjectures regarding the impact of the dual regulation of BK channels by Ca^{2+} and voltage, rather than from robust direct tests of the conditions that activate BK current in a given cell.

Rat adrenal chromaffin cells (CCs) have been one cell type in which attempts have been made to correlate aspects of the molecular and functional properties of the BK channels to excitability properties of the cells (Solaro et al., 1995; Ding et al., 1998; Sun et al., 2009). Many rat CCs express predominantly inactivating BK-type Ca^{2+}- and voltage-activated K^+ currents, termed BK_i currents (~80% of CCs), whereas other cells have largely noninactivating BK currents, termed BK_s (Solaro et al., 1995; Ding et al., 1998). The BK inactivation behavior in rat CCs is thought to arise from the variable expression of the BK β2 auxiliary subunit encoded by the *kcnmb2* gene (Xia et al., 1999). The specific inactivation properties of single BK_i channels containing one to four β2 subunits (Wang et al., 2002) has provided a quantitative framework by which it is possible, under conditions where cytosolic Ca^{2+} is robustly elevated, to infer the mean number of β2 subunits per BK channel in macroscopic BK currents in CCs (Ding et al., 1998). Mixtures of inactivating and noninactivating BK currents have also been reported in both mouse CCs (Marcantoni et al., 2010; Vandael et al., 2010) and bovine CCs (Lovell

Correspondence to Christopher J. Lingle: clingle@morpheus.wustl.edu

Abbreviations used in this paper: Ab, antibody; AHP, afterhyperpolarization; AP, action potential; CC, chromaffin cell; IP, immunoprecipitation; KO, knockout.

© 2014 Martinez-Espinosa et al. This article is distributed under the terms of an Attribution–Noncommercial–Share Alike–No Mirror Sites license for the first six months after the publication date (see http://www.rupress.org/terms). After six months it is available under a Creative Commons License (Attribution–Noncommercial–Share Alike 3.0 Unported license, as described at http://creativecommons.org/licenses/by-nc-sa/3.0/).

The Rockefeller University Press $30.00
J. Gen. Physiol. Vol. 144 No. 4 275–295
www.jgp.org/cgi/doi/10.1085/jgp.201411253

The Journal of General Physiology

Downloaded from http://rupress.org/jgp/article-pdf/144/4/275/1793887/jgp_201411253.pdf by guest on 09 February 2026

et al., 2000). Although inactivation is the most prominent functional signature of the presence of β2 subunits, to date the most significant physiological consequence of the presence of β2 subunits reflects its ability to shift gating of BK channels to more negative potentials at a given Ca^{2+} (Wallner et al., 1999; Xia et al., 1999). The presence of inactivating BK current in rat CCs has been associated with an enhanced ability of such cells to fire repetitively in response to constant current injection (Solaro et al., 1995; Lingle et al., 1996). The difference in firing has been directly related to the β2-induced shift in BK activation (Sun et al., 2009). In mouse CCs, an additional nuance of BK channel function has been suggested. In particular, specific coupling of BK channels with Cav1.3 channels has been proposed to play a critical role in pacemaking activity in mouse CCs (Marcantoni et al., 2010; Vandael et al., 2010). Whether this coupling may depend on association of Cav1.3 channels with BK channels of specific molecular composition is unknown, although BK currents in the absence of Cav1.3 appear to exhibit no inactivation (Marcantoni et al., 2010). Despite the notable presence of inactivating BK channels in CCs, the specific physiological role of BK channel inactivation in CCs, if any, also remains unknown.

Here, to gain insight into the potential physiological roles of BK channels containing β2 subunits, we report the generation of mice in which the β2 subunit has been genetically deleted. Comparison of WT and β2 knockout (KO) mouse tissues allows definition of tissues that clearly express β2 protein and also allows demonstration of β2 and Slo1 α subunit coassembly. From recordings of whole-cell BK current in WT and β2 KO CCs in adrenal slices and excised patch recordings from acutely dissociated CCs, we show that all inactivation of BK channels disappears in the absence of the β2 subunit. Moreover, CCs from β2 KO mice exhibit a reduced ability to fire repetitively in response to modest current injection. Surprisingly, β2 KO cells show a strong tendency toward slow-wave burst activity. The burst-like behavior is particularly apparent during spontaneous activity in CCs from β2 KO mice. We propose that the effect of β2 KO on firing may have unexpected consequences on basal versus evoked catecholamine secretion.

MATERIALS AND METHODS

Animal husbandry and procedures

All animal husbandry and experimental procedures were approved by and performed in accordance with guidelines of the Washington University School of Medicine in St. Louis Animal Care and Use Committee.

Generation of KO mice

The first exon of the *kcnmb2* gene containing start codon ATG (123 bp) was targeted for deletion and replaced with a LoxP/FRT bracketed construct including a neomycin selection cassette (Fig. S1 A). In the absence of exon 1 and its start codon, any residual *kcnmb2* message will not be translated. After germline transmission of chimeric mice, the F1 offspring were bred with early embryonic expression Cre mice (B6N.FVB-Tg [ACTB-cre] 2Mrt/CjDswJ; The Jackson Laboratory) to delete the targeted exon and neomycin cassette. The heterozygous β2 KO mice were then crossed with BL6 mice consecutively for 12 generations before inbreeding to generate homozygous β2 KO mice. The mice were maintained as $kcnmb2^{-/-}$ full KO's for experiments and as $kcnmb2^{+/-}$ heterozygotes in the BL6 background to maintain the KO allele. Genotyping of all mice was confirmed with PCR. Slo1 KO ($kcnma1^{-/-}$) mice were provided by A. Meredith (University of Maryland, Baltimore, MD).

To generate *kcnmb2* floxed mice, the F1 germline mice were bred with mice in which expression of codon-optimized FLP recombinase was under the control of mouse Pgk1, phosphoglycerate kinase 1 promoter (C57BL/6J-Tg(Pgk1-FLPo)10Sykr/J; The Jackson Laboratory) to eliminate the neomycin selection cassette. The *kcnmb2* floxed mouse line was bred with BL6 for at least 14 generations and was maintained to allow generation of mice with tissue-specific KO of the *kcnmb2* gene.

β2 KO mice exhibit no obvious differences from WT. Body weight was identical at 9 wk (WT: 22.9 ± 0.9 g; β2 KO: 22.4 ± 1.7 g; $n = 20$ for both group) and 54 wk (WT: 35.5 ± 3.6 g; β2 OK: 36.6 ± 2.5 g; $n = 10$ for both groups). Mean litter sizes were not different, and there was no occurrence of premature death during the first year.

RNA extraction and quantitative RT-PCR

Total RNA from mouse tissues was isolated using the RNeasy Plus Mini kit (QIAGEN) according to the manufacturer's recommendations. Before the reverse transcription, total RNA was treated to remove genome DNA with the DNA-free kit (AM1906; Applied Biosystems). Total RNA samples of human tissues were ordered from Takara Bio Inc. (Human Total RNA Master Panel II). cDNA was synthesized using the Retroscript kit (AM1710; Applied Biosystems). For the negative control groups, all components except the reverse transcription MMLV-RT were included in the reaction mixtures. Real-time PCR with specific primers (Table 1) was performed using Power SYBR Green PCR Master Mix (Applied Biosystems) under reaction conditions identical to that described previously (Yang et al., 2009). The slopes of primer efficiency equation for primer pairs used in this study were between −3.1 and −3.6, giving reaction efficiencies between 90 and 110%, which are typically acceptable for quantitative PCR assay. PCR specificity was checked by dissociation curve analysis and DNA electrophoresis. Message levels were normalized to the abundance of β-actin message in data analysis.

Preparation of total membrane proteins from mouse tissues

1 g of tissue from 8–12-wk-old male mice was homogenized on ice with a Teflon glass pestle in 5 ml of lysis buffer (50 mM sodium phosphate, 150 mM NaCl, 10 mM KCl, and 2% Triton X-100, pH 7.2) with 50 µl 1 M PMSF in acetone and 50 µl of protease inhibitor cocktail (Sigma-Aldrich). The suspension was rocked in 4°C cold room for 1 h and then centrifuged at 150,000 *g* for 30 min to spin down insoluble materials, and the supernatant was saved at −80°C.

Immunoprecipitation (IP), deglycosylation, and Western blotting

For IP, 1 ml of mouse tissue protein preparation was precleared by incubation with 15 µl TrueBlot anti–rabbit Ig IP beads (eBioscience) in a 4°C cold room for 1 h, followed by a brief centrifuging at 15,000 *g* to precipitate the beads. The supernatant was collected and mixed with 4 µg antibody (Ab) in a 4°C cold room for 2 h, followed by the addition of 50 µl TrueBlot IP beads. The mixture was rocked overnight and then centrifuged briefly to collect the beads. Beads were washed thrice and finally resuspended in 35 µl wash buffer (50 mM Na phosphate, 150 mM NaCl, 10 mM

Downloaded from http://rupress.org/jgp/article-pdf/144/4/275/1793887/jgp_201411253.pdf by guest on 09 February 2026

KCl, and 1% Triton X-100, pH 7.2). Abs used for IPs were anti-BK_{Ca} (1184–1200; Alomone Labs) and anti-Sloβ2 (KCNMB2; Alomone Labs).

N-glycanase PNGase F (Prozyme) was used to remove the N-linked glycosylated sugars of the IP products. The 35 µl IP bead suspension was sequentially mixed with 10 µl of 5× reaction buffer, 2.5 µl denaturation solution, 2.5 µl detergent solution, and 1 µl PNGase F (2.5 U/ml) and then incubated at 37°C for 1 h. For PNGase F (−) control, every component but the glycanase was included in the reaction. After deglycosylation, 12.5 µl of 5× SDS loading buffer was added to the reaction mixture to elute proteins from IP beads.

Western blots were performed as previously described (Yang et al., 2011; Zeng et al., 2011). Primary Abs were anti-Slo1 (L6/60; NeuroMab), anti-BKbeta2 (N53/32; NeuroMab), and the α tubulin Ab, mouse (GenScript). Mouse TrueBlot Ultra anti–mouse IgG HRP (eBioscience) was applied as the secondary Ab.

Acute dissociation of CCs

Adult C57BL/6 mice of around 12 wk old were killed by carbon dioxide inhalation and subsequently decapitated. CCs were dissociated as in Domínguez et al. (2012). In brief, adrenal glands were removed and immersed in ice-cold Ca^{2+}- and Mg^{2+}-free Locke's buffer containing the following (mM): 154 NaCl, 5 KCl, 3.6 $NaHCO_3$, 5 HEPES, and 11 glucose, pH 7.2. The glands were decapsulated, and the medullas were carefully separated from the cortical tissue. The medullas were digested in 200 ml Locke's solution containing 18 U/ml papain (Worthington Biochemical Corporation) for 20 min at 37°C without shaking. The tissue was washed three times with 50/50 solution of DMEM/F-12 containing 30 µM leupeptin and disaggregated by gentle passing through a 200-µl pipette tip. The resulting dissociated cells were plated in 12-mm poly-D-lysine–coated coverslips and allowed to attach for 20 min in the incubator before adding 1 ml of medium. Cells were incubated at 37°C in a water-saturated atmosphere with 5% CO_2 and used within 2–6 h after plating.

Slice preparations

Adult C57BL/6 mice of around 12 wk old were killed by CO_2 inhalation and subsequently decapitated. Adrenal glands were immediately removed and immersed in ice-cold Ca^{2+}- and Mg^{2+}-free Locke's buffer. Glands were trimmed of excess fat and embedded in 3% low gelling point agarose. Agarose was previously prepared by melting agar in Locke's buffer, followed by equilibration to 37°C. After tissue embedding, the agarose block was trimmed to ∼1-cm cubes that contained a single gland and glued to a tissue stand of a vibratome (VT 1200 S; Leica). The tissue stand was then placed in a slicing chamber filled with ice-cold extracellular solution gassed with 95% O_2/5% CO_2. Adrenal glands were sectioned into 200-µm thick slices. The slices were collected and kept in the gassed extracellular solution first at 32°C for 30 min and then at room temperature until recording. Experiments were performed within 2–6 h after slice preparation.

Electrophysiology

Recordings from either acutely dissociated CCs or cells in slices used the perforated patch methodology (Horn and Marty, 1988) of the whole-cell patch-clamp method (Hamill et al., 1981) with amphotericin as the permeabilizing agent (Herrington et al., 1995). Series resistance was typically ∼5–15 MΩ with >80% electronic compensation. Recordings from acutely dissociated cells used a HEKA amplifier, whereas slice recordings were with a Multiclamp 700B (Molecular Devices). The pipette recording solution contained (mM) 120 K-Aspartate, 22 KCl, 8 NaCl, 2 $MgCl_2$, and 10 HEPES, pH 7.4. The standard extracellular solution for dissociated cells was (mM) 140 NaCl, 5.4 KCl, 2 $CaCl_2$, 2 $MgCl_2$, and 10 HEPES, pH 7.4. For slice preparations, the extracellular solution contained (mM) 119 NaCl, 23 $NaHCO_3$, 1.25 NaH_2PO_4, 5.4 KCl, 1.5 $MgSO_4$, 2.8 $CaCl_2$, 11 glucose, 2 sodium pyruvate, and 0.5 ascorbic acid, pH 7.4.

For single channel activity recordings, patches from acutely dissociated CCs were excised into the aforementioned extracellular solution with the following pipette/extracellular solution (mM): 140 K-methanesulfonate, 20 KOH, 10 HEPES, and 2 $MgCl_2$, adjusted to pH 7.0 with methanesulfonic acid. The resulting inside-out patches allowed the perfusion of the cytosolic face with different test solutions. Currents were recorded using intracellular solutions containing either 0 or 10 µM Ca^{2+} with the following (mM): 140 K-Methanesulfonate, 20 KOH, and 10 HEPES, pH adjusted to 7.0 with methanesulfonic acid, and one of the following: 5 EGTA (for nominally 0 Ca^{2+}) or 5 HEDTA for 10 µM Ca^{2+}. Ca^{2+} solutions were calibrated with a commercial set of Ca^{2+} standards (World Precision Instruments). To remove BK inactivation, a 0 µM Ca^{2+} solution containing 0.1 mg/ml trypsin (Sigma-Aldrich) was applied for 1 min and then washed out with 10 µM Ca^{2+} for subsequent recordings. Inside-out patch currents were acquired using an amplifier Axopatch 200B (Axon Instruments) with digitization at 100 kHz and 10-kHz filtering.

TABLE 1

Primers used for real-time RT-PCR

Gene	Primer	Amplicon length
		bp
Mouse *kcnmb1* (β1)	Forward: 5′-TGCCTTTGGGTCAATGTATCAGCT-3′ Reverse: 5′-GCAATAGAATTCATGGTGCTTATA-3′	180
Mouse *kcnmb2* (β2)	Forward: 5′-CTCTACCACACGGAAGAGACCATG-3′ Reverse: 5′-ACTCTTCTGGTTTCCTTCTGGGTC-3′	168
Mouse *kcnmb3* (β3)	Mm_Kcnmb3_1_SG QuantiTect Primer Assay from QIAGEN	127
Mouse *kcnmb4* (β4)	Mm_Kcnmb4_1_SG QuantiTect Primer Assay from QIAGEN	86
Mouse *kcnma1* (Slo1)	Forward: 5′-TCTCAGCATTGGTGCCCTCGTAAT-3′ Reverse: 5′-GTAGAGGAGGAAGAACACGTTGAA-3′	127
Mouse *actb* (β-actin)	Forward: 5′-TGGAGAAGAGCTATGAGCTGCCTG-3′ Reverse: 5′-GTAGTTTCATGGATGCCACAGGAT-3′	127
Human *kcnmb2* (β2)	Forward: 5′-CTCTACCACACAGAAGAGACAATA-3′ Reverse: 5′-ACTCTTCTGGTTTCCTTCTGGGTC-3′	168
Human *actb* (β-actin)	Forward: 5′-TGGAGAAGAGCTACGAGCTGCCTG-3′ Reverse: 5′-GTAGTTTCGTGGGATGCCACAGGAC-3′	127

Downloaded from http://rupress.org/jgp/article-pdf/144/4/275/1793887/jgp_201411253.pdf by guest on 09 February 2026

Online supplemental material

The online supplemental material shows a map of the generation of the *kcnmb2* KO construct (Fig. S1), a figure showing quantitative PCR measurement of the presence of β2 message among human tissues (Fig. S2), a figure demonstrating the limitations of the use of a standard β2 monoclonal Ab for recognition of β2 from total proteins of native tissues (Fig. S3), and the utilization of phase plot (dV/dt) analysis to define the AP threshold among CCs of different genotypes (Fig. S4). Online supplemental material is available at http://www.jgp.org/cgi/content/full/jgp.201411253/DC1.

RESULTS

General of mice lacking the β2 subunit

A schematic of the floxed first exon of the *kcnmb2* (β2) subunit coding region used for generation of *kcnmb2* KO mice is illustrated in Fig. S1 A. After successful genomic incorporation of the targeted floxed *kcnmb2* exon (Fig. S1 B), mice with successful germline transmission were bred with Cre-deleter mice to generate a general *kcnmb2* KO animal. PCR reactions confirmed the presence or absence of the WT or KO allele among WT, heterozygous, or homozygous $kcnmb2^{-/-}$ mice (Fig. S1 C). A line of mice appropriate for tissue-specific KO of the *kcnmb2* mice are also being maintained (see Materials and methods).

Specific information about the loci of β2 subunit protein expression among different tissues is limited, and the availability of β2 KO mice provides an opportunity to determine definitively where BK channels with β2 subunits may be found. We first used a quantitative RT-PCR screen (Fig. 1 A) to determine tissues that are likely to be relatively enriched in β2 *kcnmb2* message and therefore candidates for tissues likely to express β2 protein. The adrenal medulla exhibited the strongest *kcnmb2* message levels, with message levels also elevated in various brain loci, lung, and trachea relative to the more weakly expressing tissues, such as heart, kidney, liver, intestine, and uterus. Slo1/*kcnma1* message was also determined from the same samples. Typically, *kcnmb2* message was present at levels ranging from 0.01 to 0.27 of that for *kcnma1*. For example, *kcnmb2/kcnma1* ratios for adrenal, adrenal medulla, cerebellum, cerebral cortex, hippocampus, retina, and trachea were 0.04, 0.18, 0.005, 0.02, 0.025, 0.15, and 0.60, respectively. For comparison, *kcnmb2* message levels were also examined in a set of human tissues (Fig. S2).

Based on those tissues with relatively higher levels of *kcnmb2* message, we next tested for the presence of β2 protein. We noted that in Western blots of total protein (Fig. S3) only poorly resolved bands were observed near the expected β2 molecular mass (27 kD for nonglycosylated protein), even when using a glycanase enzyme to remove N-linked oligosaccharides. We therefore used two manipulations to facilitate visualization of β subunit protein as performed previously (Yang et al., 2009). First, we used an initial Ab (Alomone polyclonal) to immunoprecipitate β2 from total proteins before Western blotting with a second anti-BKbeta2 Ab (NeuroMab N53/32). Second, we treated some protein samples with *N*-glycanase to remove attached sugars. Together these manipulations allowed clear visualization of bands of the expected β2 molecular weight in all tested tissues (Fig. 1 B). This band was absent in similarly isolated proteins from β2 KO mice. It should be noted that bands of molecular weight similar to the expected molecular weight of the β2 subunit were found in both WT and β2 KO tissues (Fig. S3). This points out the challenges of using existing Abs to probe the presence of β2 protein without using the glycanase procedure or having the KO control. Together, these procedures established the unambiguous presence of β2 protein in WT adrenal, adrenal medulla, hippocampus, cerebral cortex, cerebellum, spinal cord, trachea, and lung (Fig. 1 B).

We next addressed whether β2 protein may be associated with Slo1 α subunits. Total proteins from cerebellum, cerebral cortex, and adrenal medulla were immunoprecipitated with a Slo1 Ab (Fig. 2 A). This resulted in successful pull-down of β2 from WT proteins but not from proteins of $slo1^{-/-}$ or $kcnmb2^{-/-}$ mice (Fig. 2 A). This establishes that the β2 subunit and Slo1 α subunits associate in native tissues. This experiment also indicates that Slo1 protein levels are not altered in $kcnmb2^{-/-}$ mice. We also observed that β2 protein levels were markedly reduced in cerebellum, cortex, and adrenals of $slo1^{-/-}$ mice (Fig. 2 B). We conjecture that this may represent degradation of β2 protein in the absence of Slo1 α subunits. Consistent with this idea, we confirmed that *kcnmb2* message levels were unaltered in adrenals (Fig. 2 C) and cerebellum (Fig. 2 D) of the $slo1^{-/-}$ mice.

Although both the Alomone anti-BKbeta2 Ab and the NeuroMab N53/32 β2 Ab were of use for IP and identification of β2 protein in our Western blot procedures, in our hands these Abs resulted in identical staining in brain sections from both WT and β2 KO mice (not depicted). This is not surprising given the abundance of additional bands on the Western blots that are stained by these Abs (Fig. S3).

Testing for BK current inactivation in WT CCs

Most rat adrenal CCs express primarily inactivating BK currents (Solaro and Lingle, 1992; Solaro et al., 1995; Ding et al., 1998), but ∼20% of rat CCs exhibit a more sustained BK current. That these differences arise from differing intrinsic properties of the channels has been established both from inside-out single channel recordings (Solaro et al., 1995) and also from the properties of whole-cell BK current activated by depolarization with 10 µM Ca^{2+} in the recording pipettes (Ding et al., 1998). Using procedures similar to those used for rat CCs (Prakriya et al., 1996; Prakriya and Lingle, 2000), we recorded currents in acutely dissociated mouse CCs using perforated patch recording methods (Fig. 3 A). The

Downloaded from http://rupress.org/jgp/article-pdf/144/4/275/1793887/jgp_201411253.pdf by guest on 09 February 2026

standard protocol used a "Ca^{2+} loading step" by stepping to a voltage (−10 to 10 mV) that results in near maximal Ca^{2+} influx through voltage-dependent Ca^{2+} channels. A subsequent test step to 80 mV (110 mV for cells in slices) terminated Ca^{2+} influx (Van Goor et al., 2001) but then revealed strong additional BK current activation, dependent on the extent of residual Ca^{2+} elevation (Prakriya et al., 1996; Van Goor et al., 2001). Although the time course of Ca^{2+}-dependent K^+ current activated by such a procedure is influenced by several factors, including extent of Ca^{2+} elevation, Ca^{2+} clearance mechanisms, and intrinsic properties of BK channels, if sufficiently long Ca^{2+} loading steps are used, the approach provides a useful macroscopic signature of the presence of inactivating BK channels (Prakriya et al., 1996; Van Goor et al., 2001; Marcantoni et al., 2010).

In some mouse CCs, as the duration of the Ca^{2+} loading step was increased, the BK current activated at 80 mV exhibited increasingly rapid current decay (Fig. 3 A), with current decaying during the test step at 80 mV, often to a level similar to that of the current activated by a direct step to 80 mV (that is, without Ca^{2+} loading; Fig. 3, red traces). As loading step duration was increased, the peak BK current often exhibited a diminution indicative that BK channels are inactivating during the loading step. This behavior has been shown to reflect CCs in which most or all BK channels exhibit inactivation. In previous work (and see Fig. 6), the excess current activated at 80 mV after the Ca^{2+} loading step has been confirmed as BK current by its sensitivity to paxilline (Marcantoni et al., 2007) and charybdotoxin (Ding et al., 1998) and its requirement for extracellular Ca^{2+} (Marcantoni et al., 2007).

In some mouse CCs, the identical protocol resulted in currents that, as the loading step duration was increased, showed progressively weaker current decay or decay to a relatively sustained current level (Fig. 3 B). These currents also reflected BK currents as indicated

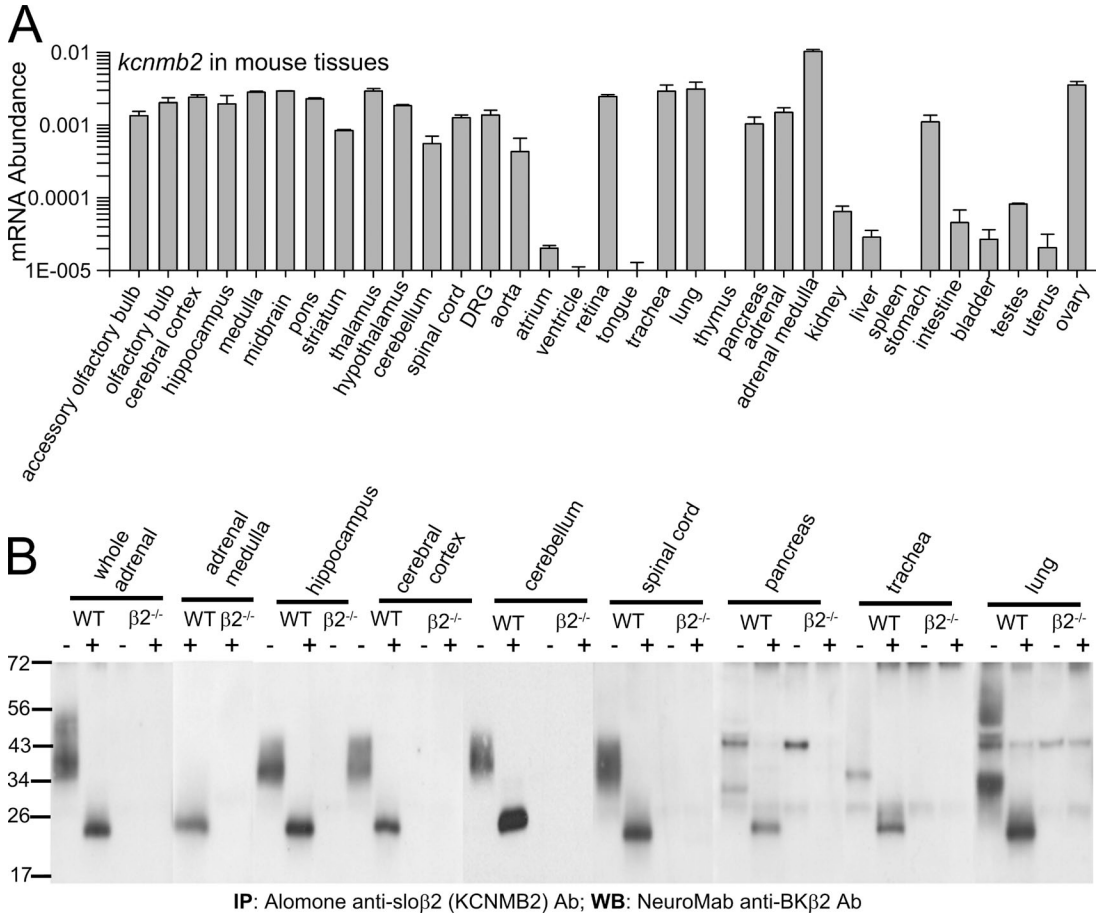

Figure 1. Distribution of *kcnmb2* message and demonstration of β2 (KCNMB2) protein in specific tissues. (A) Quantitative RT-PCR was used to define relative (normalized to β-actin) *kcnmb2* message abundance. Each estimate corresponds to mean and standard error for RNA preparations from three mice, each done in triplicate. (B) Total proteins were first immunoprecipitated with the Alomone anti-Sloβ2 Ab. Subsequently, aliquots of proteins obtained by IP were then treated with (+) or without (−) *N*-glycanase, separated by Western blot (WB), and visualized with NeuroMab anti-BKbeta2 N53/32 Ab. All tested tissues reveal β2 protein that is absent in the *kcnmb2*$^{-/-}$ mice. Note the apparent diversity of molecular size of glycosylated β2 protein among various tissues. Glycanase-free lanes were omitted for adrenal medulla because of the small size of original tissue samples. Molecular mass is indicated in kilodaltons.

Downloaded from http://rupress.org/jgp/article-pdf/144/4/275/1793887/jgp_201411253.pdf by guest on 09 February 2026

by their sensitivity to charybdotoxin (Ding et al., 1998) and their complete absence in *slo1* KO CCs (Fig. 3 G). However, such currents appeared to arise from BK channels that did not exhibit intrinsic inactivation. Because the molecular composition and physiological roles of inactivating and noninactivating BK channels differ, the comparisons in Fig. 3 point out the importance of using loading steps of sufficient duration (>200 ms) to distinguish whether the BK time course at positive potentials reflects Ca^{2+} clearance or BK inactivation. Previous work combining fluorescent Ca^{2+} buffers and current measurements in pituitary cells has nicely demonstrated the impact of loading step duration on properties of the actual Ca^{2+} elevation, as measured by fluorescent Ca^{2+} indicators (Van Goor et al., 2001). For Ca^{2+} loading steps of <50 ms in duration, Ca^{2+} clearance may be sufficiently rapid to result in BK current that decays with a time course that is characteristic of inactivating BK channels, even for channels that are intrinsically noninactivating.

Examination of BK current properties in adrenal medullary slice recordings

Below, we examine firing properties of mouse CCs from recordings in adrenal medullary slices. Therefore, to confirm that the properties of BK currents can be distinguished under slice recordings, we have also examined

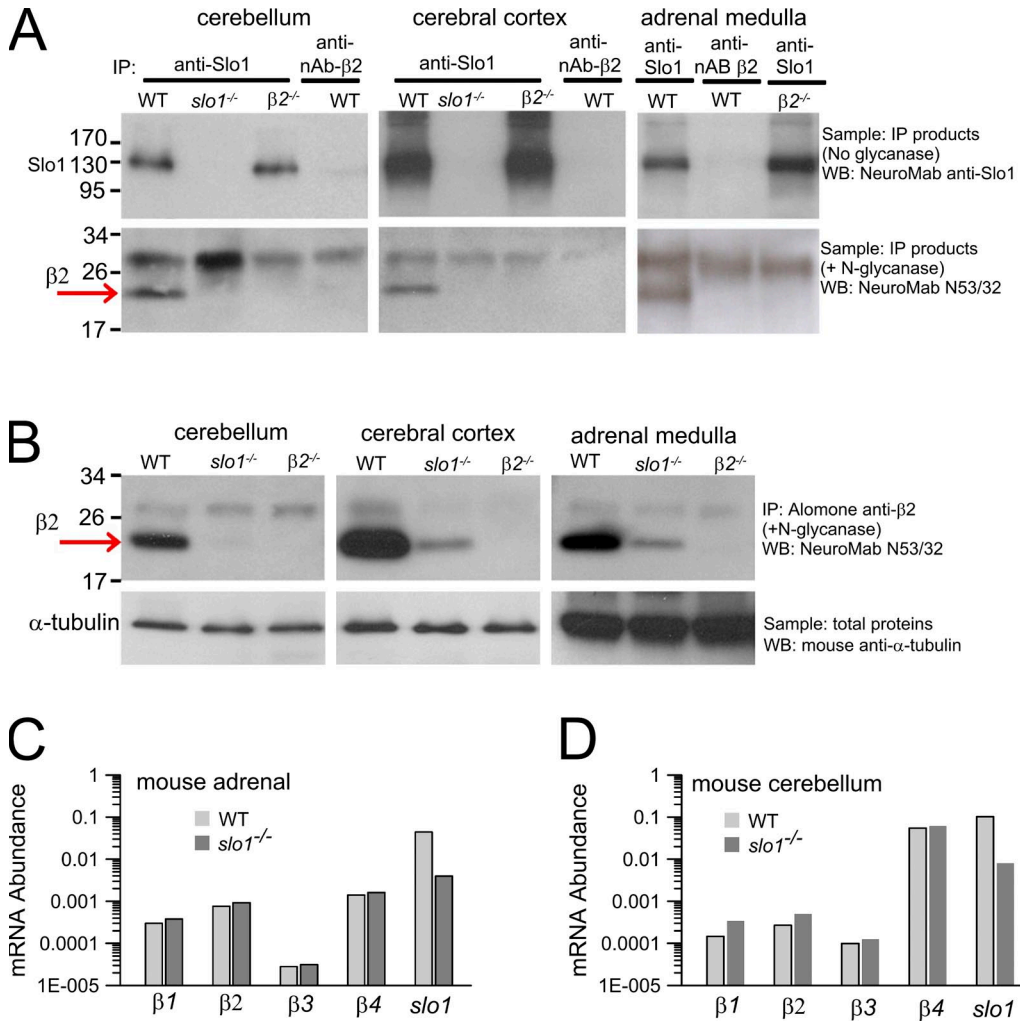

Figure 2. β2 protein co-assembles with Slo1/BK protein, but in the Slo1 KO, β2 protein, but not β2 message, is diminished. (A) Total proteins were initially immunoprecipitated with NeuroMab anti-Slo1 Ab or the NeuroMab N53/32 BKβ2 Ab (nAB) and then visualized either with NeuroMab N33 Slo1 Ab (top) or with NeuroMab BKβ2 N53/32. Slo1 protein is unaffected by KO of the β2 protein in all tested tissues (top), whereas β2 (red arrow) is markedly reduced after KO of Slo1 (bottom). nAb-IP, which corresponds to omission of Ab during IP but inclusion of IP beads, is ineffective at IP of either Slo1 or β2. The bottom panels establish that, in WT tissues, IP of Slo1 also pulls down β2 protein. (B) Total proteins from the indicated tissues and genotypes were initially immunoprecipitated with Alomone anti-BKbeta2 Ab, treated with *N*-glycanase, and then visualized with NeuroMab anti-BKbeta2 N53/32. β2 protein (red arrow) is markedly reduced in tissues from *slo1*$^{-/-}$ mice and totally absent in tissues from *kcnmb2*$^{-/-}$ mice. (A and B) Molecular mass is indicated in kilodaltons. WB, Western blot. (C) Relative mRNA abundance in mouse adrenal (whole adrenals) from one WT and one Slo1 KO mouse was determined in triplicate for β1, β2, β3, β4, and Slo1, with normalization to β-actin message. (D) Relative abundance of different subunits for WT and *slo1*$^{-/-}$ mice is shown for cerebellum.

Downloaded from http://rupress.org/jgp/article-pdf/144/4/275/1793887/jgp_201411253.pdf by guest on 09 February 2026

the properties of macroscopic BK currents using the protocols just presented. As with acutely dissociated cells, mouse CCs in slices exhibited a range of behaviors in regards to BK current inactivation (Fig. 3, C and D). Some fraction of cells exhibited BK current that inactivates essentially completely (Fig. 3 C), whereas other cells exhibited only weak inactivation or sustained BK current (Fig. 3 D). For comparison with our earlier work with cultured rat adrenal CCs (Solaro et al., 1995; Lingle et al., 1996), we also undertook perforated patch recordings from rat CCs in slices. As in mouse, we observed cells with either marked inactivating BK current (Fig. 3 E) and other cells that exhibited little or no BK current inactivation (Fig. 3 F). Finally, for CCs from mice with KO of the *kcnma1* Slo1 gene, the same stimulation protocols failed to elicit any Ca^{2+}-dependent current, irrespective of the Ca^{2+} loading step duration (Fig. 3 G).

From the currents activated by the protocol of Fig. 3, we determined several aspects of the evoked currents. The parameters measured are schematized in Fig. 4 A for a mouse CC with inactivating BK current and in Fig. 4 B for a mouse CC with largely noninactivating BK current. First, from the direct step to 110 mV, we measured peak outward current (I_{Kv}), which reflects primarily voltage-dependent K^+ current. Although some activation of BK current by voltage alone might contribute to such current, the inability of paxilline to reduce such current (see below) suggests that the I_{Kv} is almost exclusively Kv current. Second, we measured peak inward current during the loading step to 10 mV. Third, we measured the largest peak outward current elicited by the family of loading steps. The difference between the peak outward current and the persistent I_{Kv} was taken to provide a minimal estimate of the maximal BK current in the cell. Fourth, we measured the current that persists at the end of the test depolarization to 110 mV after the longest loading step. The amount of the persistent current after subtraction of the Kv component allowed estimation of the fractions of inactivating or noninactivating BK current. Finally, we measured the time constant of decay of the BK current after the longest loading step duration. Although in cells with inactivating BK current this time constant in part reflects the mean number of β2 subunits per channel in the channel population, Ca^{2+} clearance rates may also impact the decay of BK current, particularly in cells with noninactivating currents. However, as a relative measure of the underlying properties of BK currents among different cells, the time constant of decay after a strong Ca^{2+} loading step provides a useful measure of the inactivation behavior of the channel population.

From the above measurements in CCs from mouse slices, the time constants of BK current decay exhibited a broad distribution (Fig. 4 C). 45% (18 of 40) of the cells exhibited almost complete current decay with a time constant of <110 ms, whereas the others showed incomplete and slower current decay. On average, rat CCs from slices exhibited a narrower distribution of time constants of decay, with most cells (85%; 17 of 20) exhibiting decay time constants of <110 ms. This is consistent with the view that rat CCs express, on average, BK channels containing a higher mean number of β2

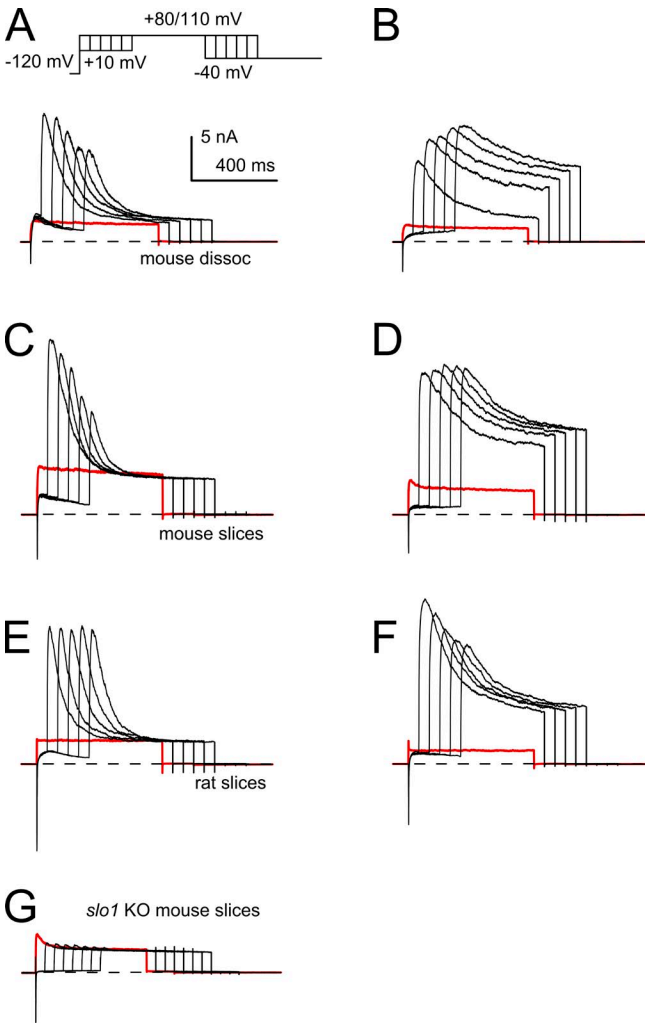

Figure 3. Tests of whole-cell inactivating BK current in mouse CCs. (A) The indicated voltage protocol was used to elicit current during perforated patch recordings. As the duration of a loading step to 10 mV is increased, peak outward current during the step to 80 mV is progressively reduced and current decays almost completely to a level identical to that evoked by voltage alone. This defines a cell with largely inactivating BK current. (B) In another dissociated mouse CC, increases in the loading step duration result in increasingly diminished current decay during the step to 80 mV. This reflects largely noninactivating BK current (right). The red traces highlight the direct step to 80 mV from −120 mV, reflecting primarily Kv current. (C) Traces show currents from a mouse CC from adrenal medullary slices with inactivating BK current. For cells in slices, the positive test step was to 110 mV. (D) Traces show a mouse CC in a slice with largely noninactivating BK current. (E) Traces show a rat CC in a slice with largely inactivating BK current. (F) Traces highlight a mostly noninactivating BK current in a rat CC from a slice. (G) Traces from a *slo1* KO CC illustrate the absence of a current dependent on a Ca^{2+} loading step.

Downloaded from http://rupress.org/jgp/article-pdf/144/4/275/1793887/jgp_201411253.pdf by guest on 09 February 2026

subunits per channel, resulting in somewhat more robustly inactivating BK currents. The relationship between the BK current decay time constant and the fraction of sustained BK current in a cell also highlights the range of properties of BK currents among mouse CCs (Fig. 4 D). For mouse CCs, with a decay time constant of ~110 ms or faster (red symbols), the fraction of sustained BK current is consistently less than ~0.05, whereas for mouse CCs that decay with time constants slower than 110 ms, the persistent BK current ranges from 0.05 to near 1.0. For these cells with slower current decay, because some of this decay may reflect Ca^{2+} clearance rates, the estimates of persistent BK current probably underestimate the actual noninactivating BK current.

These results indicate that, among different mouse CCs, BK channels exhibit a broad range of properties possibly consistent with a differential expression of the β2 subunit among CCs. Furthermore, CCs with strongly inactivating BK currents appear to occur less frequently in mouse adrenals compared with rat adrenals. Based on the present results (and see Fig. 7), we suggest that mouse CCs express BK channels which, on average, have fewer β2 subunits per channel than is usually observed in rat CCs.

We place importance on understanding, at least qualitatively, the distribution of behaviors of BK currents in the CC population for the following reason. The mean number of β2 subunits per BK channel in a cell is hypothesized to impact the range of voltages over which the BK channels may function at a given Ca^{2+} concentration. The presence of β2 subunits also influences BK current activation rates, with β2-containing channels opening more slowly than channels lacking β2 (Orio et al., 2006). This in turn will dictate the effect that BK channels will have on firing in a given cell. Therefore, as a tool for assessing how BK currents of different phenotypic properties may impact cell firing, we have somewhat arbitrarily separated the mouse CCs studied here into two populations, using a cut-off time for the decay time constant of 110 ms to separate cells that are more strongly inactivating from those with weaker or absent inactivation. For convenience, we retain the earlier terminology of BK_i for CCs that exhibit inactivating BK current and BK_s for those with noninactivating current. However, it is probably more accurate to view the properties of BK currents in the mouse CC population (and perhaps rat) as a continuum of behaviors between inactivating

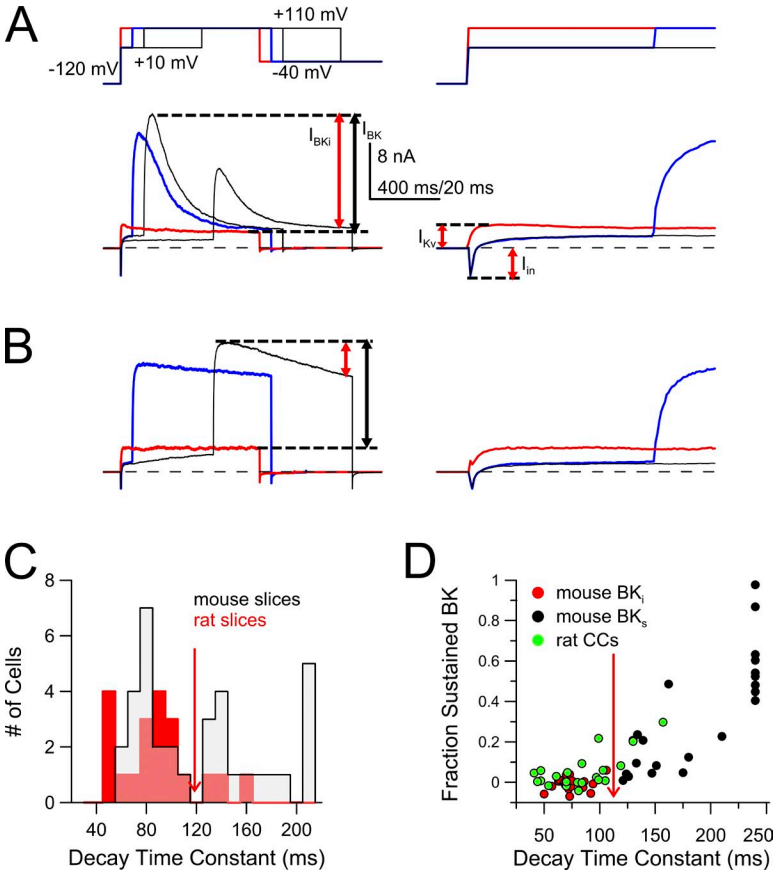

Figure 4. Definition of current components. (A) Traces on left show currents from a mouse CC in a slice with largely inactivating BK currents. The first two traces highlight the peak current activated by a direct step to 110 mV (red trace) and then the additional outward current activated by the step 110 mV after a 50-ms loading step to 10 mV (blue trace). Longer loading steps result in larger outward current at 100 mV. Black arrows show maximal total amount of current that activates as a consequence of the Ca^{2+} loading step to 10 mV above that activated by a direct step to 80 mV (red trace). Red arrows identify the fraction of that current that is inactivated by this protocol. On the right, the first two traces on an expanded time base highlight the peak current activated by a direct step to 110 mV (red trace; I_{Kv}) and the net inward current activated by a step to 10 mV (blue trace; I_{in}). (B) Traces show currents from a mouse CC with predominantly noninactivating BK current. The red arrow highlights the fraction that may inactivate (but which may also reflect Ca^{2+} clearance). (C) Frequency distribution of current decays from mouse (black) and rat (red) CCs recorded in slices is plotted as a function of decay time constant. Time constants were fit to the decaying phase of current after the longest loading step in the family of traces (as in A and B). The red arrow highlights an arbitrary point separating the more rapidly and more slowly decaying currents in mouse. In mouse, 45% of cells had BK currents decaying faster than 110 ms. In rat, 85% of cells decayed faster than 110 ms. (D) The decay time constants from cells as in C are plotted as a function of the fraction of sustained BK current in the same cell, as defined from the current that persists (red arrows in A and B). The red arrow in D defines the arbitrary separation of cells with largely inactivating current (BK_i) and largely noninactivating current (BK_s) used here.

Downloaded from http://rupress.org/jgp/article-pdf/144/4/275/1793887/jgp_201411253.pdf by guest on 09 February 2026

and noninactivating (Fig. 5 A). Based on the definitions just provided, we compared peak BK current (Fig. 5 B), peak inward current at 10 mV (Fig. 5 C), and peak outward current at 110 mV (I_{Kv}; Fig. 5 D) among all mouse CCs, mouse BK_i CCs, mouse BK_s CCs, and rat CCs, all from slice recordings. The only significant difference was that rat CCs exhibited significantly smaller voltage-dependent K^+ current density than mouse CCs, as has been previously noted (Marcantoni et al., 2010). CCs from Slo1 KO mouse exhibited peak inward and I_{Kv} similar to that in WT CCs, but no outward current dependent on the Ca^{2+} loading step (Fig. 5, C and D).

KO of β2 removes inactivation of BK current in mouse CCs

We next examined properties of BK currents in mouse CCs from β2 KO animals. In a set of 22 cells from adrenal medulla slices from β2 KO animals, no cells exhibited any sign of inactivation using the protocols that revealed BK inactivation in WT CCs. Whereas loading steps in many WT mouse CCs exhibited robust activation of a paxilline-sensitive inactivating BK current (Fig. 6, A and B), similar loading steps in CCs from β2 KO mice activated a completely noninactivating, but paxilline-sensitive outward current (Fig. 6, C and D). The peak BK current activated in the β2 KO cells generally exceeded those of WT cells, probably indicative that the presence of β2 subunits reduces peak current either from persistent steady-state inactivation or inactivation during the rising phase of current activation. These results confirm that the inactivation of BK channels in mouse CCs arises from the β2 auxiliary subunit. For comparison, CCs from BK KO mice exhibited no K^+ current dependent on a Ca^{2+} loading step (Fig. 6 E) and no paxilline-sensitive current (Fig. 6 F).

We next examined excised inside-out patches from dissociated CCs from either WT or β2-KO mice. Most patches from WT CCs expressed primarily inactivating BK channels (Fig. 7, A′ and B′), which were confirmed as BK channels by their Ca^{2+} dependence (Fig. 7, A″ and B″) and unitary current levels. However, there was considerable variation in the time constants of decay of the ensemble mean currents. Because the mean number of β2 subunits in a BK channel influences not only inactivation, but the mean V_h for channel activation at a given Ca^{2+} (Wang et al., 2002), we generated G-V curves for sets of patches that differed in the mean time constants of inactivation. To allow measurement of peak current activation without any confounding effect of inactivation, the G-V curves were generated from currents after removal of inactivation by trypsin. For patches with, on average, faster inactivating channels, the G-V curve approached that characteristic of heterologously expressed mSlo1 + β2 (Fig. 7 A‴). For patches with more slowly inactivating channels, the averaged G-V was somewhat flattened and shifted to the right (Fig. 7 B‴). We then examined excised inside-out patches from β2

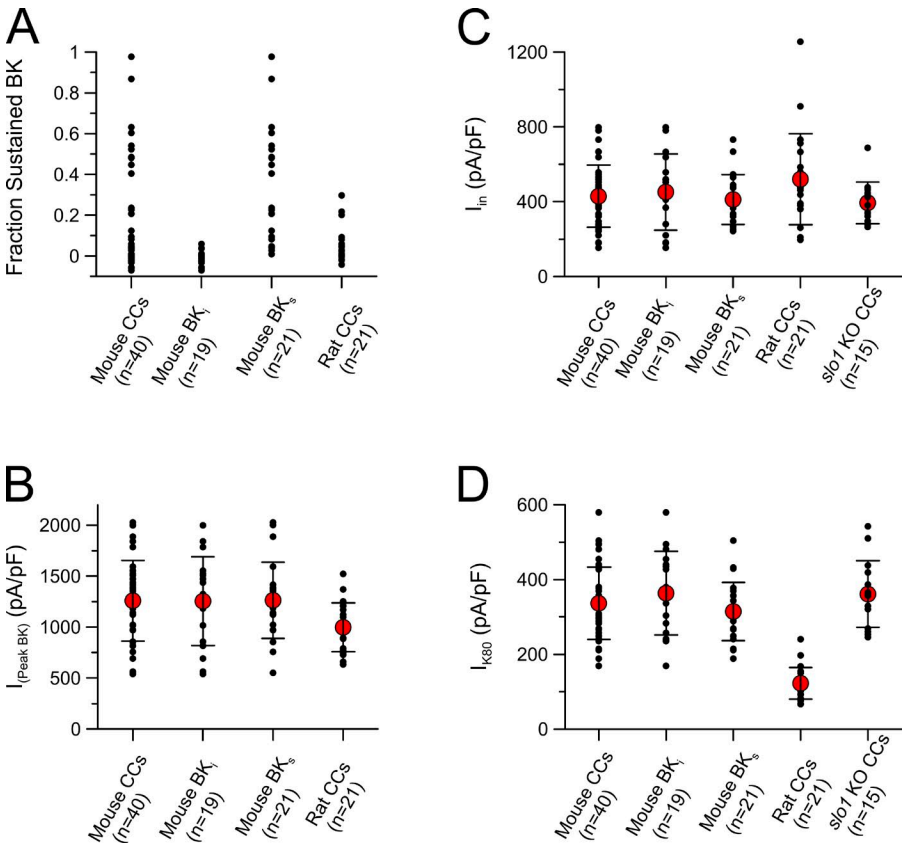

Figure 5. Comparison of current components among mouse BK_i and BK_s CCs and rat CCs. (A) The fraction of persistent BK current at the end of a 600-ms step to 80 mV after a several hundred–millisecond Ca^{2+} loading step to 10 mV is plotted for all mouse CCs (in slices) and then those defined as having largely BK_i current or largely BK_s current, along with the results from 21 rat CCs (in slices). (B) Mean (±SD) values for the maximal BK current density are displayed for each group of cells along with the individual values. No statistically significant differences were observed. (C) Mean (±SD) values of peak inward current observed after the initial step to 10 mV are displayed for each group of cells and also included 15 *Slo1* KO CCs. (D) Mean (±SD) values of peak outward current during direct steps to 110 mV for each group of cells (including *Slo1* KO). This current largely reflects Kv current, and rat CCs differ from mouse CCs with $P < 0.001$ (*t* test).

Downloaded from http://rupress.org/jgp/article-pdf/144/4/275/1793887/jgp_201411253.pdf by guest on 09 February 2026

KO CCs. For five patches, no inactivating BK channels were ever observed (Fig. 7, C′ and C″), and the resulting G-V curve was comparable with that obtained for heterologous expression of mSlo1 alone. For 30 patches from WT CCs, we plotted the distribution of numbers of patches with ensemble currents of a given inactivation time constant (Fig. 7 D). The overall mean inactivation time constant was 46.6 ± 18.8 ms (SD). Based on earlier work with heterologously expressed α + β2 subunits and assuming that a channel with four β2 subunits inactivates with an ~20-ms time constant (Wang et al., 2002), this would suggest that most BK channels in mouse CCs contain, on average, approximately one to two β2 subunits per channel, which is somewhat less than previously estimated from rat cells (Ding et al., 1998). For the set of 30 inside-out patches, we determined there to be a total of 196 inactivating channels and 32 noninactivating BK channels. Assuming random assembly of β2 and α subunits with five potential stoichiometries with a 0.15 fraction of channels with no β2 subunits, the binomially predicted fraction of channels with one, two, three, and four β2 subunits would be 0.362, 0.333, 0.136,

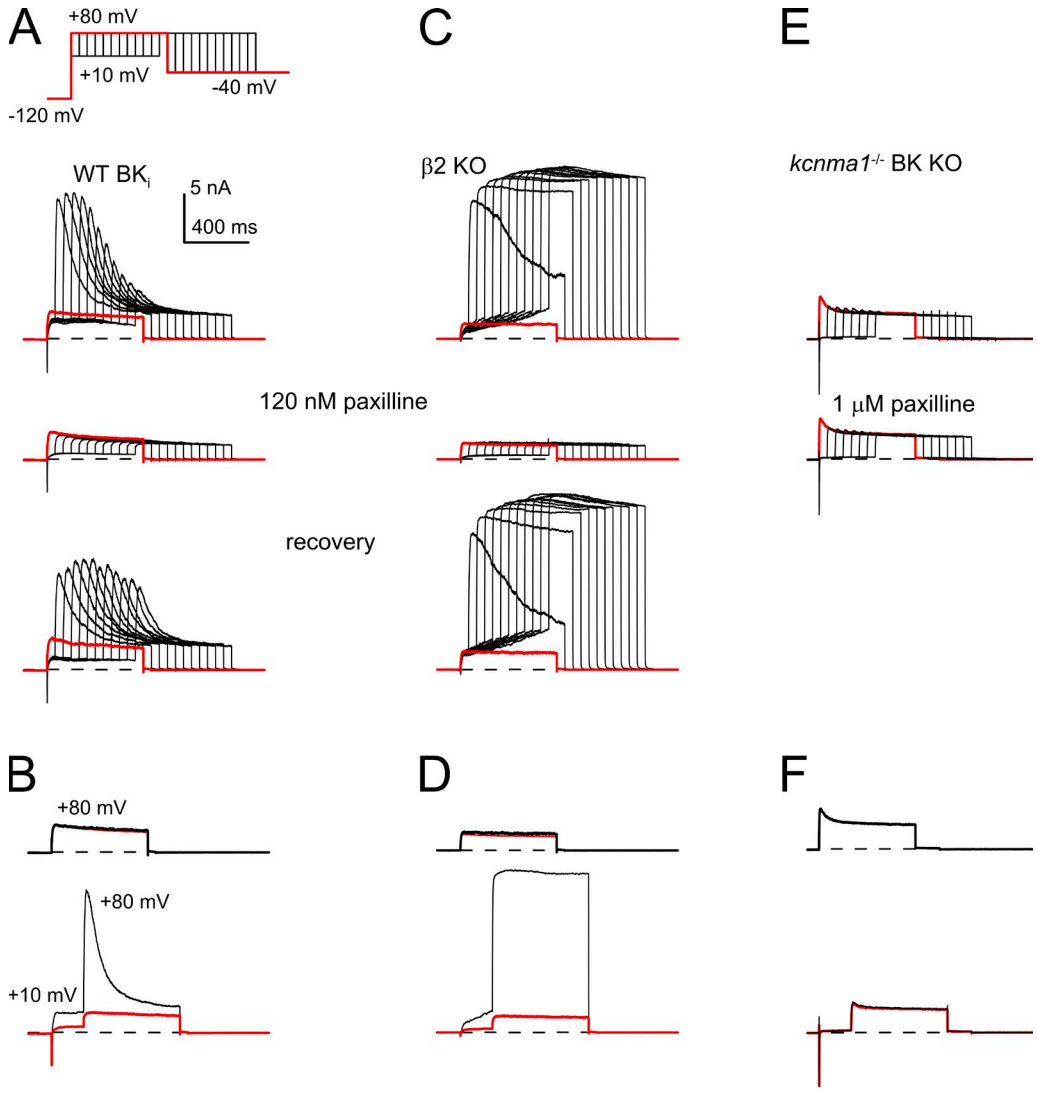

Figure 6. Inactivating BK currents are absent in CCs from *kcnmb2*$^{-/-}$ mice. (A) The indicated voltage protocol was used to elicit currents in a dissociated mouse CC to establish the presence of BK$_i$ currents. In the middle, 120 nM paxilline removed all current activated at 80 mV that was dependent on the loading step to 10 mV. Washout of paxilline reversed the inhibition. (B) Selected traces from A before (black) and in the presence of 120 nM paxilline (red; obscured in top example by control trace) show currents evoked by direct step to 80 mV (top) and then currents at 80 mV after a Ca^{2+} loading step to 10 mV. (C) The identical protocol was used on a dissociated CC from a β2 KO mouse, showing the strong paxilline sensitivity and reversibility of the noninactivating BK current. (D) Traces highlight the robust noninactivating paxilline-sensitive BK current in a CC from a β2 KO mouse. (E) Traces show currents from a CC from a *slo1*/BK KO mouse, without and with 1 μM paxilline. (F) Traces from the *slo1*/BK KO example in E, showing the absence of paxilline effect on currents elicited either by a direct step to 80 mV (top; red trace in paxilline is obscured by control trace) or after a Ca^{2+} loading step (bottom).

Downloaded from http://rupress.org/jgp/article-pdf/144/4/275/1793887/jgp_201411253.pdf by guest on 09 February 2026

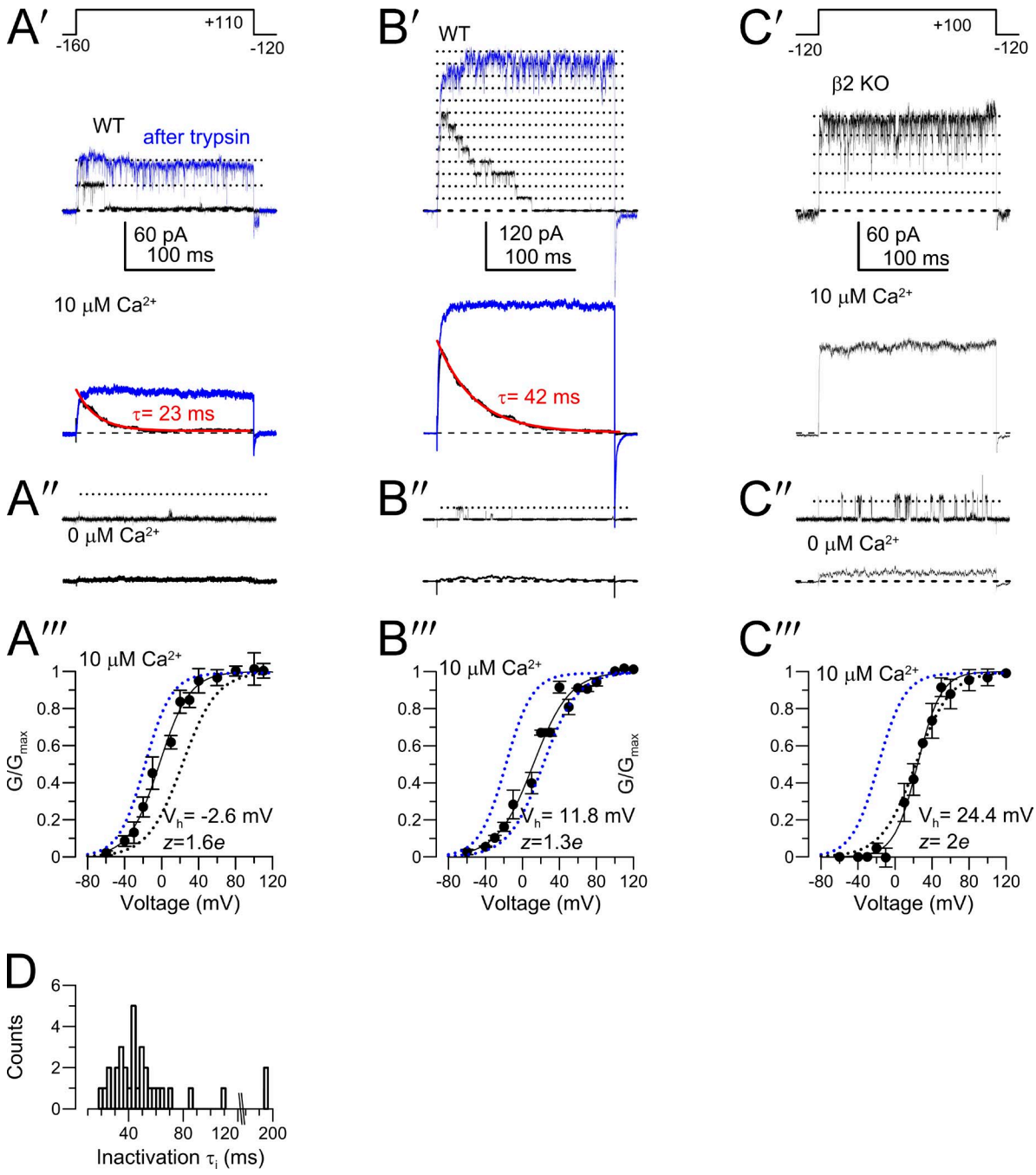

Figure 7. Single BK channels in CCs from *kcnmb2*$^{-/-}$ mice do not inactivate. (A′) Channel openings in a patch from a WT CC were activated with the indicated voltage protocol with 10 μM cytosolic Ca^{2+}. Top traces show single channel sweeps before and after (blue trace) brief application of trypsin to remove inactivation. Bottom traces show means of 20 sweeps before and after trypsin, with a single exponential (red) fit to the inactivation time course. (A″) Traces show a single sweep and a mean of 20 for the patch at the top, but with 0 Ca^{2+}. Scale bar applies to A′ and A″. (A‴) A G-V curve was generated from BK channel activation (after removal of inactivation) for two cells with mean ensemble inactivation time constants of <35 ms. A fitted Boltzmann yielded the values shown on the figure. Dotted lines correspond to mean G-Vs at 10 μM Ca^{2+} for Slo1 alone and Slo1 + β2, when expressed heterologously in oocytes. (B′) Top traces show channel openings from a patch from another WT CC, before and after removal of inactivation. Bottom traces are means of 20 sweeps before and after removal of inactivation, along with the fitted exponential (red). (B″) Traces correspond to a single sweep (top) and the mean of 20 sweeps with 0 μM Ca^{2+}. Scale bar applies to B′ and B″. (B‴) The points reflect an averaged G-V curve for four patches with ensemble inactivation time constants between 42 and 49 ms. Dotted lines are as in A‴. (C′) Traces shows openings elicited with 10 μM Ca^{2+} in a patch from a *kcnmb2*$^{-/-}$ CC. (C″) Trace shows ensemble mean of 20 sweeps from the patch at the top. (C‴) A G-V curve for BK channels from three patches from *kcnmb2*$^{-/-}$ CCs. Error bars indicate SEM. (D) The frequency distribution of numbers of patches from WT cells having a given inactivation time constant is shown. Bin to the right of the break in the x axis highlights two patches with entirely noninactivating BK channels.

Downloaded from http://rupress.org/jgp/article-pdf/144/4/275/1793887/jgp_201411253.pdf by guest on 09 February 2026

and 0.021. This also predicts a mean stoichiometry of 1.52 β2 subunits per channel. Having defined the variation in properties of BK currents and other currents in native mouse CCs, we now examine firing properties of CCs from WT and KO mice.

β2 KO CCs exhibit spontaneous bursting

We begin with an examination of the spontaneous firing behavior in WT and β2 KO cells in slices, using the perforated patch recording method. We noted three general categories of firing behavior among CCs of different

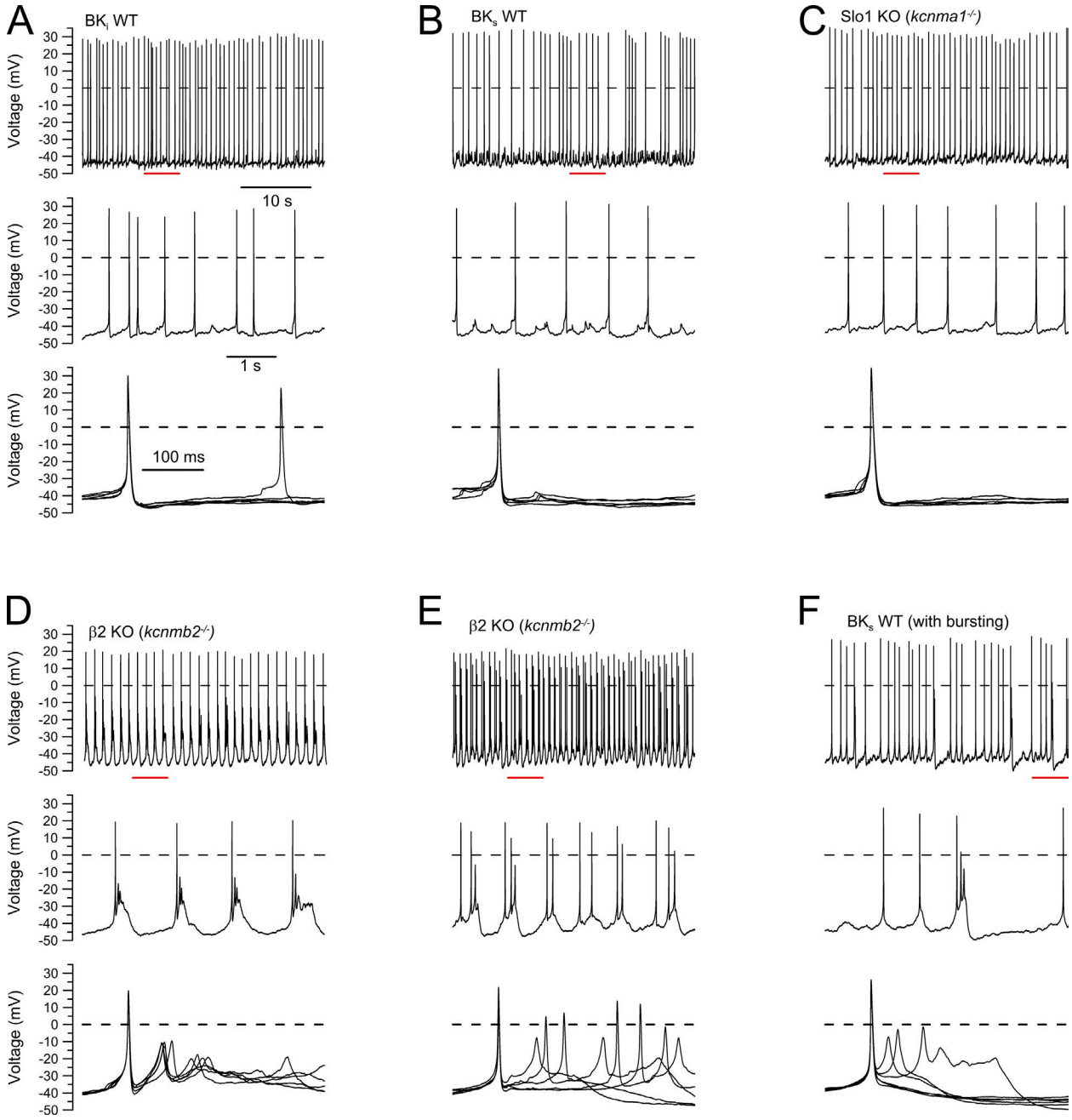

Figure 8. Spontaneous APs occur in bursts in CCs from β2 KO mice. (A) Traces show spontaneous firing from WT mouse CCs expressing inactivating BK current. Top trace shows 35 s of continuous activity, middle trace shows 5 s of activity on a faster time pace (red segment on top trace), and the bottom shows a set of eight APs aligned on the time point at which the AP reaches 0 mV. (B) Traces show spontaneous activity from a CC with largely noninactivating BK (BK$_s$) current. (C) Traces show spontaneous APs from a CC from a *kcnma1*$^{-/-}$ mouse. (D) Traces show bursting, slow-wave activity from a CC from a *kcnmb2*$^{-/-}$ mouse. (E) Spontaneous activity from another *kcnmb2*$^{-/-}$ CC. (F) Traces illustrate spontaneous activity in a WT CC with primarily noninactivating BK current, in which occasional slow-wave burst activity was observed. All recordings are from cells in adrenal medullary slices.

Downloaded from http://rupress.org/jgp/article-pdf/144/4/275/1793887/jgp_201411253.pdf by guest on 09 February 2026

types. First, in many cells, persistent spontaneous firing occurs at a mean frequency around 1 Hz. Second, some cells were largely quiescent, firing APs intermittently or at mean frequencies of <0.2 Hz. Third, we observed some cells that exhibit a tendency toward slow-wave activity associated with bursts of APs. WT cells with predominantly inactivating BK current typically exhibited a persistent firing of single APs at around 1–2 Hz (Fig. 8 A), whereas WT cells with predominantly noninactivating BK current also exhibited persistent spontaneous firing at around 1 Hz (Fig. 8 B), but with a higher likelihood of cells that were largely silent. CCs from Slo1 KO animals also exhibited spontaneous firing of similar frequency (Fig. 8 C), but with a higher percentage of cells that were largely silent. In general, these firing behaviors of WT mouse CCs in slices are similar to those previously observed for dissociated WT mouse CCs (Marcantoni et al., 2010). In marked contrast to either the WT or the Slo1 KO cells, in most CCs from β2 KO animals, spontaneous firing generally consisted of brief bursts of a single full AP followed by lower-amplitude APs riding on a plateau potential (Fig. 8, D and E). Similar bursting behavior was also noted to occur, although only intermittently, in some WT cells with relatively noninactivating BK current (Fig. 8 F).

The distribution among relatively quiescent, repetitively firing, and bursting cells differed among the three groups of cells (Fig. 9 A; BK_i, BK_s, and β2 KO). For the BK_i cells, burst firing was never observed and ∼68% of all cells exhibited repetitive spontaneous firing. For the BK_s cells, more than half the cells were largely quiescent and fired at overall frequencies <0.2 Hz. However, a small set of BK_s cells exhibited some tendency to burst firing. For the β2 KO cells, almost 80% of all cells exhibited a tendency toward burst firing. The frequency of such bursts was similar to the frequency of the spontaneous APs in the WT cells (Fig. 9 B). Most Slo1 KO cells exhibited only intermittent firing, with ∼40% of cells exhibiting some repetitive firing.

β2 KO slows AP repolarization and reduces AHP after single APs

Inhibition of BK channels prolongs AP duration and reduces AHPs in both rat (Solaro et al., 1995) and mouse chromaffin (Vandael et al., 2010) cells, but the specific impact of the BK current on AP properties most likely depends on the presence of β2 subunits (Sun et al., 2009). We therefore compared the properties of individual APs in CCs in slice recordings from WT and β2 KO mice. Under current clamp, we attempted to maintain a mean holding potential of −50 mV and we evoked single APs with a 5-ms, 150-pA (or 250 pA) step. Two different injection currents were examined because in some cells the 5-ms, 150-pA injection only slowly elicited an AP. For each cell, an averaged AP was generated from 5–20 individual APs (focusing on APs that arose from a −50-mV holding potential). The means from individual cells were then averaged for each group of cells. We first compared averaged APs elicited by either 150 or 250 pA current injections for those WT CCs categorized as having predominantly BK_i current (Fig. 10 A). Not unexpectedly, the larger injected current resulted in a faster time to peak AP, although there was little difference in the peak amplitude of the AP. The larger injected current also resulted in a more pronounced AHP after the AP, although the falling phase of the APs over most of the AP time course was similar. The more pronounced AHP with stronger current injection likely reflects a stronger activation of BK current, as this AHP is blocked by paxilline (not depicted). For comparison between APs, we measured the membrane voltage at 15 ms after the AP peak, which for the BK_i cells corresponded closely with the most negative excursion of the AHP. A similar comparison of APs evoked in β2 KO cells with two levels of injected current revealed a somewhat

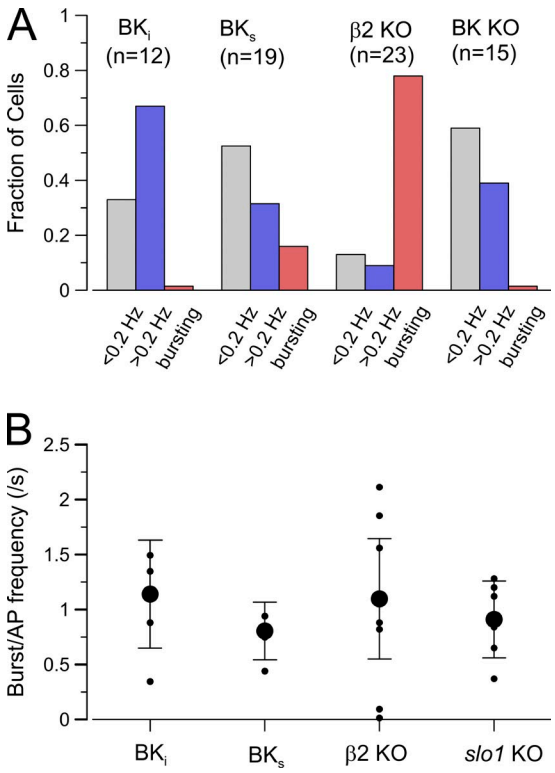

Figure 9. β2 KO CCs are more likely to exhibit burst firing. (A) Frequency distribution among three firing behaviors are plotted for BK_i (n = 12 cells, left), BK_s (n = 19 cells, middle-left), β2 KO (n = 23 cells, middle-right), and *slo1* KO (n = 15 cells, right). Spontaneous activity was typically evaluated for a period of 150 s. Firing categories were as follows: 1, APs at a total frequency of <0.2 Hz (this includes quiescent cells in which APs could be evoked by depolarization); 2, repetitively firing APs at a frequency of >0.2 Hz; and 3, repetitive firing in which full-size APs precipitated burst firing. (B) AP firing frequency for BK_i, BK_s, β2 KO, and *slo1* KO cells. Cells firing at <0.2 Hz were not included. For β2 KO cells, each burst was considered as a single event. Error bars indicate SEM.

Downloaded from http://rupress.org/jgp/article-pdf/144/4/275/1793887/jgp_201411253.pdf by guest on 09 February 2026

larger peak AP, but only small differences during repolarization, suggesting that the BK current is similarly activated in response to both current injections (Fig. 10 B).

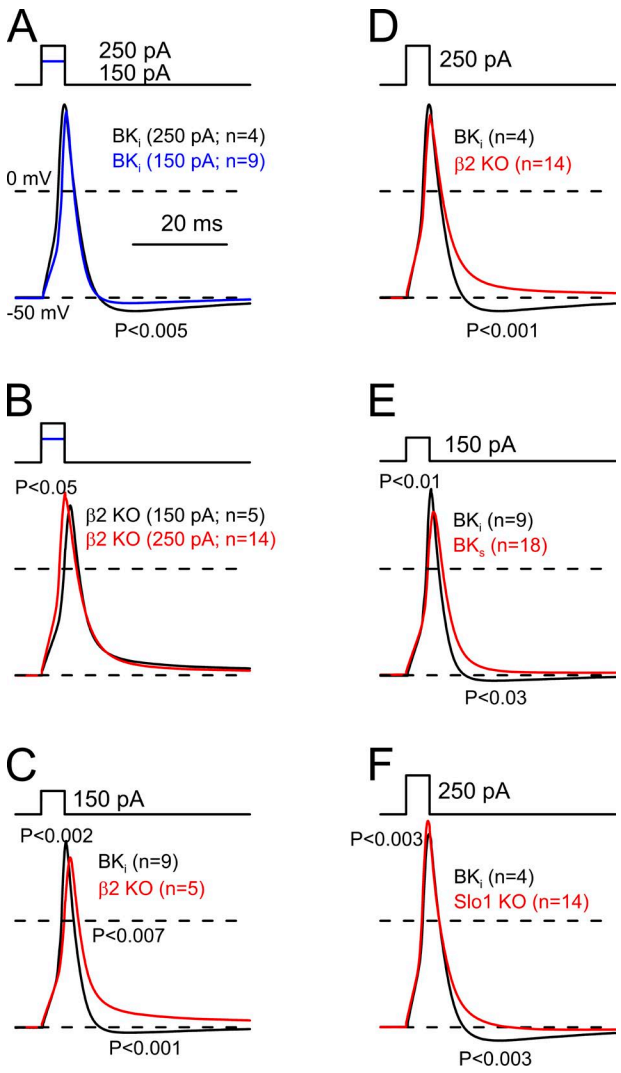

Figure 10. Single evoked APs in CCs without β2 subunits exhibit slowed repolarization and an absence of AHP. (A) The indicated injected current pulse (5 ms for 150 [or 250] pA) was used to elicit single APs in CCs in slices. For each cell, an averaged AP was generated from 3–10 individual APs. The averaged AP from each cell was then averaged with those from other cells, with *n* as indicated. APs are from sets of BK$_i$ cells stimulated either with a 150-pA pulse (blue trace) or 250 pA pulse (black). The voltage reached during the AHP was significantly more different with the 250-pA pulse. (B) APs are compared for sets of β2 KO cells stimulated either with a 150 (black)- or 250-pA (red) pulse. The 250-pA AP exhibits a larger peak amplitude. (C) APs are compared for BK$_i$ and β2 KO cells stimulated with a 150-pA pulse. β2 KO cells exhibit a smaller peak amplitude and pronounced depolarizing afterpotential. (D) APs are compared for BK$_i$ and β2 KO cells stimulated with a 250-pA pulse. The depolarizing afterpotential is even more pronounced. (E) APs are compared for BK$_i$ and BK$_s$ cells, showing a smaller peak AP amplitude and reduced AHP in the BK$_s$ cells. (F) APs are compared for BK$_i$ and Slo1 KO CCs, showing a larger peak amplitude and slower repolarization in the Slo1 KO cells.

It should be noted that these brief 5-ms current injections did not elicit any secondary AP spikes after the initial evoked AP. Direct comparison of the APs elicited by 150-pA current injection in BK$_i$ cells with that in β2 KO cells (Fig. 10 C) reveals that the peak amplitude of the AP in β2 KO cells is reduced and repolarization is markedly slowed, both during the AP falling phase and times corresponding to the AHP. The difference in AHP is even more pronounced between WT BK$_i$ and β2 KO cells after a 250-pA injection (Fig. 10 D).

In general, the difference in AHP properties between WT BK$_i$ and β2 KO cells can be explained by the idea that, in the β2 KO cells, the shift in gating of the BK channels to more positive potentials results in less BK channel activation during the repolarizing phase of current in the β2 KO cells. However, this alone is unlikely to explain the rather sustained persistence of the membrane potential at values more positive than the initial holding potential in the β2 KO cells.

Given the idea that BK$_s$ cells may contain, on average, fewer β2 subunits per BK channel and have many BK channels that may lack β2 subunits entirely, we compared APs evoked in WT BK$_i$ cells with those in WT BK$_s$ cells (Fig. 10 E). Similar to effects observed with β2 KO, the peak AP was reduced in the BK$_s$ cells and the AHP was diminished, although not quite as much as observed in β2 KO cells. Thus, qualitatively, the behavior of the BK$_s$ cells approaches that of the β2 KO cells. A comparison of the individual estimates of AP peak and AHP amplitude for BK$_i$ versus BK$_s$ cells (Fig. 11, A and B) indicates that the BK$_s$ cells exhibit considerable more variability than observed for those categorized as BK$_i$. Possible reasons for this are considered in the Discussion. Finally, we compared the BK$_i$ AP with that observed in CCs from Slo1 KO mice (Fig. 10 F). In contrast to the reduced amplitude of the APs observed in the BK$_s$ and β2 KO CCs, the Slo1 KO CCs exhibited a larger peak AP amplitude. Repolarization proceeded similarly to that in BK$_i$ cells until potentials negative to 0 mV, at which point repolarization was slowed in the Slo1 KO cells, although not as much as in the β2 KO cells. The mean values and individual estimates of peak AP amplitude (Fig. 11, A, D, and G), AHP amplitude (Fig. 11, B, E, and H), and AP duration (Fig. 11, C and F) are compared for the different cell types in Fig. 11. Qualitatively, the slower repolarization and reduction of AHP in the β2 KO cells is consistent with the expected weaker BK activation in the absence of the β2 subunit, whereas the slow repolarization in the Slo1 KO cells is also consistent with that idea. However, the fact that repolarization occurs even more slowly in β2 KO cells than Slo1 KO cells seems surprising, given that β2 KO cells still retain a BK current. Although future work is required to address this point, given the tendency of β2 KO cells to exhibit slow wave bursting activity, we postulate that the balance of currents in β2 KO cells somehow maintains

Downloaded from http://rupress.org/jgp/article-pdf/144/4/275/1793887/jgp_201411253.pdf by guest on 09 February 2026

a persistent inward current that contributes to the sustained depolarization and tendency to burst.

A limitation of the use of a constant current pulse to elicit APs is that the stimulus itself will result in activation of voltage-dependent channels with a time course different than what would occur with naturally occurring APs. Therefore we also compared the properties of aligned spontaneous APs from each category of cell. APs were aligned based on the time of the AP peak. As above, we averaged a set of APs from each individual cell and then averaged these among a set of cells. A comparison of BK_i versus β2 KO APs (Fig. 12 A) reveals differences qualitatively similar to those seen for the evoked APs. The β2 KO cells exhibit a smaller AP peak and a sustained depolarization during the time the BK_i cells exhibit an AHP. For the β2 KO cells, some of the sustained depolarization in fact reflects contributions of cells in which burst activity follows the initial AP. When WT BK_i and BK_s spontaneous APs are compared (Fig. 12 B), this also reveals differences similar to those seen for evoked APs. Namely, BK_s APs exhibit a reduced AHP. Finally, a comparison of the WT BK_i AP with the

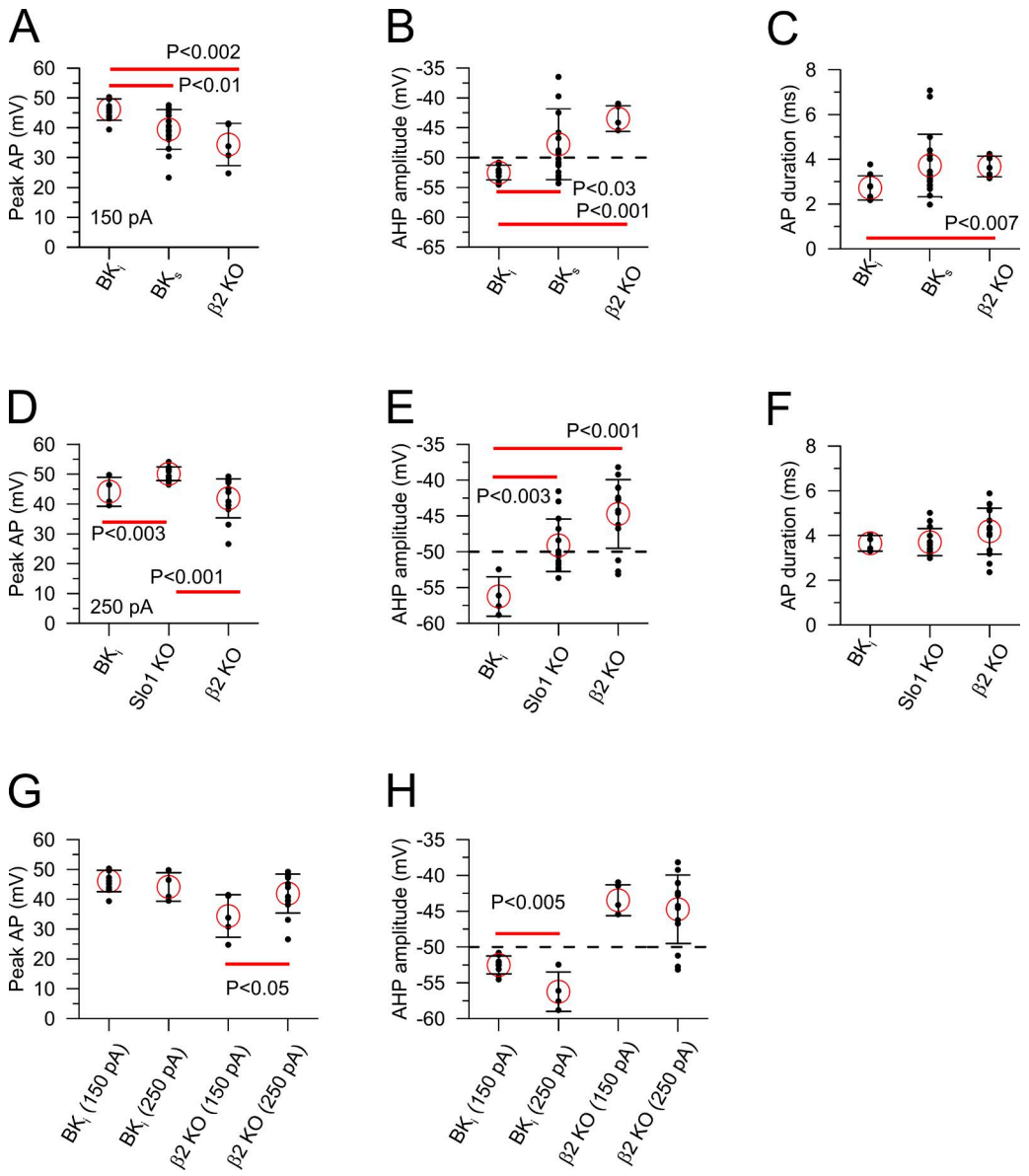

Figure 11. Properties of evoked single APs. (A) Mean (red circles) and individual values of peak AP amplitude are shown for BK_i, BK_s, and β2 KO cells. Errors are SD. Differences were evaluated with a *t* test statistic. A–C use 150-pA current injection. (B) The membrane voltage at the time of the peak AHP in the BK_i cells was determined for BK_i, BK_s, and β2 KO cells. The dotted line at −50 mV indicates the holding potential. (C) AP durations (duration at half peak AP) are plotted for BK_i, BK_s, and β2 KO cells. (D) Peak AP amplitudes are compared for BK_i, Slo1 KO, and β2 KO cells. D–F use 250-pA current injection. (E) AHP amplitudes are compared for BK_i, Slo1 KO, and β2 KO cells. (F) AP durations are compared for BK_i, Slo1 KO, and β2 KO cells. (G) Peak AP amplitudes are compared for BK_i and β2 KO at both the 150- and 250-pA injections. (H) AHP amplitudes are compared for the 150- and 250-pA injections for BK_i and β2 KO cells.

Downloaded from http://rupress.org/jgp/article-pdf/144/4/275/1793887/jgp_201411253.pdf by guest on 09 February 2026

Slo1 KO AP (Fig. 12 C) shows a slowing of the repolarization in the Slo1 KO AP similar to that observed in the evoked APs, although the slowing seems more pronounced in the spontaneous APs. To test for potential differences in AP threshold in the different types of cells, we generated plots of dV/dt for the averaged APs from each cell (Fig. S4). For each cell the maximum dV/dt was determined. Although AP threshold is largely an arbitrary determination, we defined AP threshold as the membrane potential at which dV/dt reaches 4% of the maximum dV/dt for a given cell. This measure has been used previously both in mouse CCs (Vandael et al., 2012) and in a study of pacemaking in dopaminergic neurons (Khaliq and Bean, 2010). Based on this measure, the AP threshold did not differ between BK_i, BK_s, and β2 KO cells, whereas the Slo1 KO cells exhibited a slightly high threshold (Fig. S4 and Table 2). Peak dV/dt was reduced in β2 KO cells relative to the other cell types. Measurements of resting potential and input resistance over the range of −60 to −70 mV did not reveal any differences among each type of cell (Table 2) and resulted in values similar to those observed in other studies.

A principal difference between the evoked APs and the spontaneous APs is in the peak amplitudes of the APs. The peak AP amplitude resulting from injected current is typically over 40 mV for all cell types and even closer to 50 mV in the Slo1 KO cells, whereas for spontaneous APs, the mean peak AP is at least 10 mV more negative. This presumably reflects weaker and more gradual voltage-dependent Na^+ (and Ca^{2+}) channel activation in the spontaneously firing cells given their somewhat more positive resting potentials. At more negative peak APs, this is likely to result in larger net Ca^{2+} influx thereby favoring more robust Ca^{2+} influx during the spontaneous APs in comparison with the evoked APs. This might, in part, contribute to the more marked effect of the Slo1 KO on spontaneous AP repolarization than seen in the evoked APs. Additional work will be required to sort out the contributions of different current components during physiological AP waveforms.

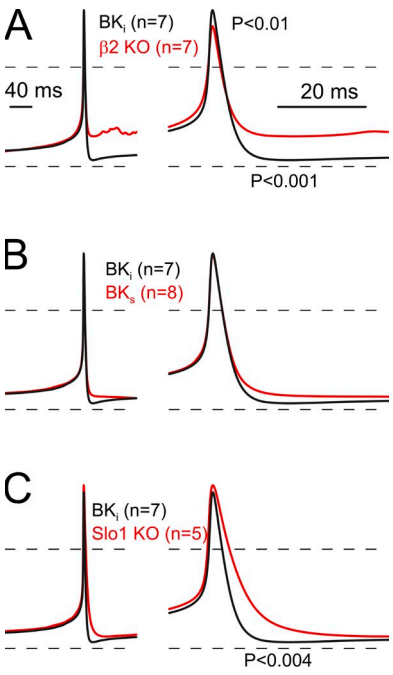

Figure 12. Spontaneously occurring single APs in β2 KO CCs exhibit slowed repolarization and persistent afterdepolarizations. (A) Traces are averaged spontaneous APs for BK_i and β2 KO (red) CCs. APs from individual cells were aligned on the time of peak AP potential. β2 KO cells exhibit reduced peak AP amplitude and a pronounced depolarizing afterpotential. (B) Traces compare spontaneous APs in BK_i and BK_s, revealing a reduced AHP in the BK_s cells. (C) APs from BK_i and Slo1 KO CCs are shown, revealing a larger peak amplitude and prolonged repolarization phase in the Slo1 KO cells.

Comparison of AP firing elicited by smaller, sustained current injection

We also examined the ability of WT mouse CCs to fire repetitively during 2-s constant current injections of different magnitude. For each WT cell, a measure of the macroscopic BK current behavior was first obtained from a prolonged Ca^{2+} loading step and a subsequent step to 110 mV to determine whether the cell had weaker or more robust inactivation, as shown in Fig. 13 A (right hand traces) for a BK_i cell and Fig. 13 B (right hand traces) for a BK_s cell. Consistent with earlier observations from rat CCs (Solaro et al., 1995), cells with inactivating BK current are better able to support higher-frequency firing at stronger current injection (Fig. 13, A vs. B at 20-pA injection and E). Similar procedures were used in CCs from β2 KO animals (Fig. 13 C). In comparison with WT cells with more strongly inactivating BK current, these β2 KO cells (n = 22) uniformly exhibited weaker firing in response to the stronger levels of constant current injection (Fig. 13 E). Intriguingly, at the smaller levels of injected current, β2 KO cells exhibited a tendency toward slow-wave activity and bursts of APs (Fig. 13 C). CCs from Slo1 KO cells were also able to support higher firing frequencies (Fig. 13 D) and did not exhibit spontaneous burst behavior, but were less effective at firing repetitively at more modest current injections (Fig. 13 E). Overall, these results show that the presence of BK channels containing the β2 subunit is an important factor in sculpting how mouse CCs fire in response to depolarization.

DISCUSSION

The present work establishes the successful generation of mice lacking expression of KCNMB2/β2 protein. For initial validation of the consequences of β2 KO, we have exploited mouse CCs. The results definitively confirm that the β2 subunit does, in fact, underlie inactivating BK channels in CCs. As predicted from earlier considerations

Downloaded from http://rupress.org/jgp/article-pdf/144/4/275/1793887/jgp_201411253.pdf by guest on 09 February 2026

TABLE 2

Electrical parameters defined for spontaneously firing CCs

Cell type	r.p.	R_{in} −60 to −70 mV	V_{thresh} dV/dT (4%)	Peak AP	$dV/dt_{(max)}$
	mV	*GΩ*	*mV*	*mV*	*V/s*
BK_i	−43.1 ± 1.8 (6)	1.6 ± 0.8 (10)	−27.1 ± 1.9[a] (8)	29.9 ± 6.3[b] (7)	60.6 ± 26.1[a] (8)
BK_s	−43.8 ± 1.7 (6)	1.7 ± 0.5 (12)	−26.3 ± 2.0 (8)	28.1 ± 7.8 (8)	52.9 ± 21.8 (8)
β2 KO	−43.2 ± 2.3 (6)	1.9 ± 1.3 (12)	−26.7 ± 1.6 (9)	20.1 ± 4.4[b] (7)	32.0 ± 15.7[a] (9)
Slo1 KO	−44.4 ± 2.1 (4)	1.9 ± 2.2 (12)	−24.5 ± 2.0[a] (5)	32.2 ± 5.8 (5)	51.8 ± 11.0 (5)

[a]$P < 0.05$.
[b]$P < 0.01$.

of differences in firing between rat CCs with largely inactivating BK current and those with more sustained BK current (Solaro et al., 1995; Sun et al., 2009), the absence of the β2 subunit reduces the ability of mouse CCs to fire repetitively during constant current injection. However, two aspects of our results were not expected based on earlier work. First, CCs from β2 KO mice exhibit spontaneous slow-wave burst firing. Second, after single APs evoked by strong depolarizing current pulses, β2 KO cells exhibit a persistent afterdepolarization. Here we discuss the role of β2 subunits in CCs and other cells and then address the more speculative topic of how burst firing may arise in the β2 KO cells.

The role of BK channels containing β2 subunits

In rat adrenal CCs, inactivating (BK_i) and noninactivating (BK_s) macroscopic BK currents are largely segregated among different cells with ∼75% of the rat cells exhibiting an almost completely inactivating BK current (Solaro et al., 1995; Ding et al., 1998), whereas additional cells exhibit BK currents with slower or absent inactivation. The properties of both the macroscopic

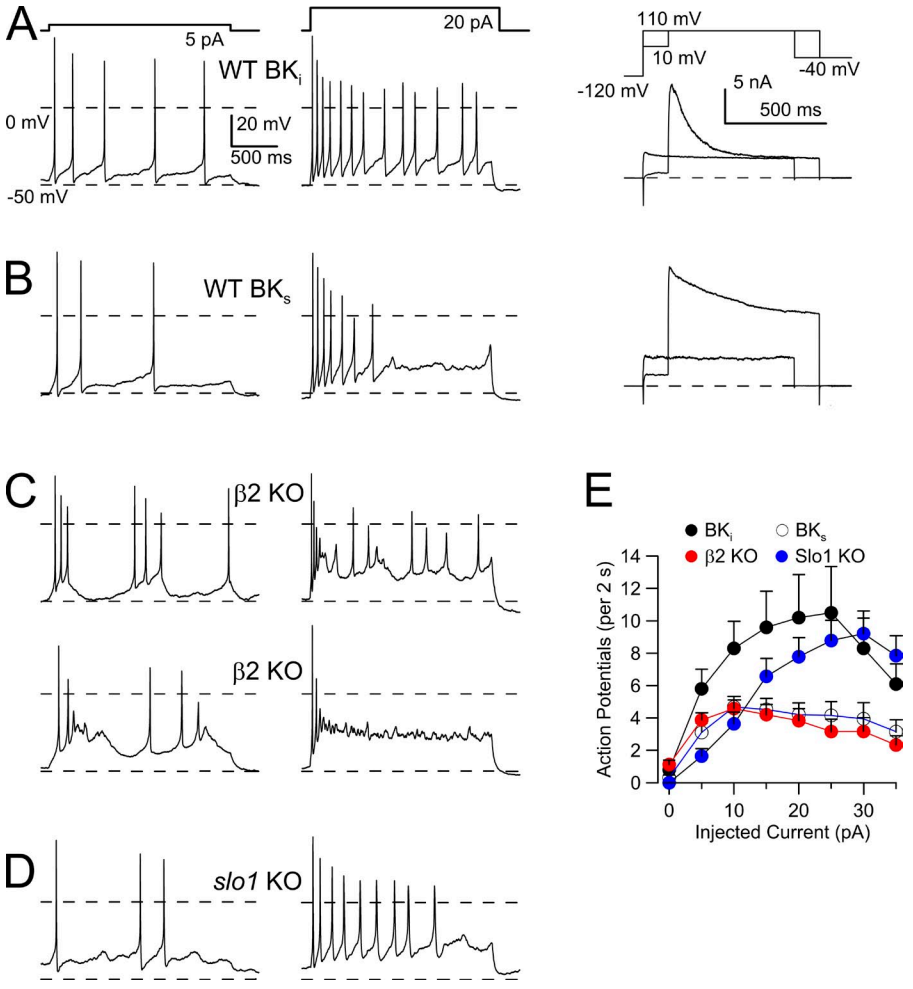

Figure 13. Absence of β2 subunits reduces frequency of APs evoked by constant current injection and predisposes to burst firing. (A) AP firing was elicited by either a 5 (left)- or 20-pA (middle) constant current pulse in a CC with BK_i current (confirmed with the protocol and traces on right). (B) AP firing was elicited in a BK_s cell (sample traces on right) with either 5- or 20-pA current pulses. (C) Two examples of CCs in adrenal slices from β2 KO mice are shown both with 5 (left)- and 20-pA (right) current injection. Note the slow-wave activity with bursts of spikes at 5 pA. (D) A *slo1* KO CC is displayed for 5- and 20-pA current injections. (E) The mean (±SD) number of evoked APs (excursions above 0 mV) is plotted as a function of injected current amplitude for the four cell types.

Downloaded from http://rupress.org/jgp/article-pdf/144/4/275/1793887/jgp_201411253.pdf by guest on 09 February 2026

and single BK channels in rat CCs are generally consistent with the properties conferred on BK channels by the β2 auxiliary subunit, message for which is present in rat adrenals (Xia et al., 1999). In addition to inactivation, the β2 subunit also shifts the gating range of the resulting BK channels to more negative potentials at a given $[Ca^{2+}]$. Although a potential physiological role of inactivation per se has not as yet been determined, the ability of β2 subunits to shift gating has been proposed and modeled as a plausible explanation for the ability of rat CCs to sustain repetitive firing during constant current injection (Sun et al., 2009), compared with cells that may lack β2 subunits. Specifically, a stronger contribution of BK current to AP repolarization and AHPs in cells with the β2-shifted BK current helps promote recovery of Na^+ channels from inactivation, thereby permitting subsequent AP firing.

Through evaluation of the variation in BK inactivation among the mouse CC population, the present results further validate the idea that the relative amount of β2 subunits in the BK population within a mouse CC impacts the ability of those CCs to fire repetitively during depolarizing stimuli. Furthermore, the results with β2 KO CCs confirm the hypothesis that the gating shifts produced by the β2 subunit are critical to defining the firing properties of CCs (Sun et al., 2009). However, there are some notable differences between mouse and rat CCs. First, on average, BK current in mouse CCs appears to inactivate more slowly than in rat cells, and a larger percentage of mouse CCs appear to exhibit little or only weak inactivation of BK current. Based on inactivation time constants of BK channel ensemble means in inside-out patches, we estimated that mouse BK channels contain, on average, ∼1.5 β2 subunits per channel. Using the fraction of single noninactivating BK channels in the set of excised patches, we calculated a similar mean number of β2 subunits per channel. This compares to estimates of 2.2–2.5 from rat CCs (Ding et al., 1998). Second, mouse CCs express about twofold larger net voltage-dependent K^+ current. Our estimates of total Kv current based on the direct voltage step to 110 mV do not provide any information about the identity of Kv currents in the mouse cells. However, this current is likely to be minimally contaminated by BK current activated by voltage in the absence of Ca^{2+} because paxilline has little effect on this current. The weaker inactivation of BK current in mouse cells, meaning fewer β2 subunits and a more positive gating range, and the larger Kv current will together reduce the net impact of BK current in AP repolarization in mouse CCs relative to that in rat CCs. This is, in fact, consistent with earlier work (Vandael et al., 2010) showing that paxilline produces a much more pronounced prolongation of AP duration in rat CCs compared with mouse cells, a result we have also confirmed (unpublished data). Overall then, the present results clearly establish a critical role for β2-containing BK channels in the regulation of AP firing in mouse CCs, and we would expect that β2-containing BK channels would play an even more important role in rat CCs.

In addition to their presence in CCs, inactivating BK currents have also been described in several other cell types, including pancreatic β cells (Li et al., 1999), amacrine cells in the retina (Grimes et al., 2009), cells in the lateral amygdala (Faber and Sah, 2003), hippocampal neurons (Hicks and Marrion, 1998; Shao et al., 1999), rat dorsal root ganglion neurons (Li et al., 2007), and mouse inner hair cells (Pyott et al., 2004). Except for pancreatic β cells and perhaps dorsal root ganglion neurons, the biophysical properties of the BK currents in most of these systems have not been sufficiently defined to assess whether they clearly match with the known properties conferred on BK channels by β2 subunits. For example, although it has been proposed that β2 subunits mediate an inactivation of BK currents observed in amacrine cells in the retina (Grimes et al., 2009), the rates of inactivation and range of voltages over which inactivation is observed do not appear consistent with inactivation mediated by any known BK auxiliary subunit.

The availability of the β2 KO animals will now allow definitive tests for the presence or absence of β2-containing BK channels in any given cell system. Our results also indicate that currently available β2 Abs can be of use for identification of protein isolated from native tissues, but only when coupled with BKβ2 KO control samples.

Potential origins of bursting behavior in β2 KO CCs

The most unexpected aspect of the properties of the β2 KO cells was the very reliably observed slow-wave, burst-like activity. Such behavior was not observed in any WT CCs with predominantly inactivating BK current and only rarely observed in 3 of 20 WT BK_s cells. The underlying frequency of the bursts was quite similar to the predominant AP firing rates in WT BK_i cells, perhaps suggesting that the drivers for the onset of a burst in β2 KO cells and the BK_i APs may be similar. Bursting behavior does not appear to be typical for CCs, but does appear to be elicited with various manipulations that affect the balance of available currents. In one earlier paper using cultured mouse CCs, burst behavior was observed in a "small fraction of cells" (Marcantoni et al., 2010), perhaps similar to what we observe in WT BK_s cells. It has also been observed that 20 mM TEA, which would completely block BK but also most SK current, resulted in some burst-like activity in mouse CCs in slices (Nassar-Gentina et al., 1988). Furthermore, another study, which noted a reduction in spontaneous firing in Slo1 KO cells (Vandael et al., 2010), also reported that Cav current activation by BayK 8644 promoted bursting. Recent work from the Carbone group also suggests that manipulations that influence Na^+ current

Downloaded from http://rupress.org/jgp/article-pdf/144/4/275/1793887/jgp_201411253.pdf by guest on 09 February 2026

availability may also induce bursting in mouse CCs (Carbone, E., personal communication). It remains unclear whether these phenomena result from similar or distinct underlying burst generation mechanisms. However, the idea that bursting behavior in CCs may be unmasked by any of a variety of manipulations raises the possibility that endogenous mechanisms regulating various ion channels may lead to naturally occurring conditions that permit such bursting behavior.

The present results provide no definitive insight into why removal of β2 subunits should lead to bursting activity, and future work will be required to address this problem. However, some speculation on this topic and its relationship to bursting in other cells is warranted. The fact that bursting is observed in the β2 KO cells, not in the BK_i cells, and only rarely in BK_s cells indicates that the presence of a BK current, but with a relatively positive gating range (absence of β2 subunit), is somehow required to produce burst firing. Our estimates of the mean numbers of β2 subunits per BK channel suggest that, even in cells with relatively sustained BK current, most BK channels will probably have at least one β2 subunit. Because each β subunit in a channel shifts BK gating in an incremental fashion (Wang et al., 2002), even in a cell categorized as BK_s, the gating range of the BK channels will be somewhat shifted relative to that found in β2 KO cells. The differences between the β2 KO and BK_s cells suggest that even small differences in the gating range of the BK channel population may have effects on the ability to produce burst firing. Our results also allow the conclusion that, for the bursting we have observed in mouse CCs, BK channels lacking β2 subunits are absolutely required. Simply deleting BK channels, as in the Slo1 KO, does not support bursting.

Attention to the properties of both the evoked and spontaneous single APs also suggests additional factors that may contribute to differences in firing, resulting from β2 subunit KO. Both the evoked APs in BK_s and β2 KO cells reach smaller peak current amplitudes than in the BK_i cells. The APs in Slo1 KO cells have an even larger peak amplitude. It is well established that, in addition to its gating shifts, the β2 subunit slows BK channel activation (and deactivation; Orio et al., 2006). Thus, the differences in the peak AP amplitude may reflect the extent to which BK channels are activated during the rising phase of the AP. Without β2 subunits, BK channels arising from the α subunit alone activate rapidly, although to a lower mean open probability, during the initial AP upswing. Cells lacking any BK current at all (Slo1 KO CCs) exhibit the largest peak AP, consistent with a complete absence of BK activation during the AP upswing. The peak amplitude of the AP would, in turn, influence several other processes that would impact AP shape: the rate of Na^+ channel inactivation, the extent of Ca^{2+} influx through Ca^{2+} channels, and the extent of activation of Kv current. Experiments that examine the contributions of different current components during different AP clamp waveforms will be required to tease this apart.

The most curious aspect of the AP waveforms is the relative persistence of a depolarized afterpotential in the β2 KO cells. The afterpotential in the β2 KO cells is clearly more depolarized than that in the Slo1 KO cells. Obviously the depolarized afterpotential cannot be sustained by a K^+ current alone, but requires that some persistent inward current be active during this period. Such an inward current, poised in balance with an outward current, would potentially provide the basis for a plateau potential upon which a burst of APs could occur. For β2 KO cells to exhibit such activity, whereas the BK_s and Slo1 KO cells not show burst firing, would require either that the necessary inward current not be activated during the AP or be deactivated more rapidly. Because both BK_s and Slo1 KO CCs tend to repolarize more slowly than BK_i cells, it is not immediately clear what the key difference might be that would sustain the persistent afterdepolarization in β2 KO cells.

Mouse CCs express two types of L-type Ca^{2+} channels, Cav1.2 and Cav1.3 (Vandael et al., 2013), which may differentially couple to BK channels (Marcantoni et al., 2010). Cav1.3 channels have been proposed to act in conjunction with BK channels as the pacemaking currents that drive spontaneous firing rates in mouse CCs (Marcantoni et al., 2010). If a Cav current were driving the depolarizing afterpotential in the β2 KO cells, it would probably require that the properties of the AP result in more robust Cav activation than in WT cells. Another possibility that must always be considered when dealing with a KO animal model is that, perhaps, there is some change in expression in some other current component, e.g., Cav1.2 or Cav1.3 (Vandael et al., 2013). Although we see no obvious changes in either peak inward current or voltage-dependent outward current, we have not directly tested for differences in Cav currents between WT and β2 KO mice.

Another consideration that will impact CC firing is the well-known presence of Ca^{2+}-dependent K^+ channels of small conductance (SK channels), which have been described in both rat (Neely and Lingle, 1992) and mouse CCs (Vandael et al., 2012). In rat, the differential role of inactivating and noninactivating BK channels in influencing evoked firing frequencies is present during the complete inhibition of SK channels by apamin (Solaro et al., 1995). However, in mouse CCs, SK inhibition increases spontaneous firing frequency and SK channels play a clear role in adaptation during depolarization-evoked firing (Vandael et al., 2012). To what extent differences in SK expression among different CCs may contribute to differences in spontaneous firing rates remains unknown. It will also be important to evaluate the role SK channels may play, if any, in regulating burst durations in the β2 KO CCs.

Downloaded from http://rupress.org/jgp/article-pdf/144/4/275/1793887/jgp_201411253.pdf by guest on 09 February 2026

A previous study on bursting behavior in rat pituitary somatotrophs (Van Goor et al., 2001) may be relevant to the underlying burst mechanisms here. In such cells, which contain BK channels lacking auxiliary subunits, rapid BK channel activation during the rising phase of an AP reduces Kv activation, thereby allowing more persistent inward current activation to support a plateau potential. Adding a BK current component to a model cell transformed the cell from spontaneous firing to bursting (Van Goor et al., 2001). The rapid activation of BK current implied by the reduction in peak AP amplitude in the β2 KO cells may point to a similar mechanism in mouse CCs.

Potential physiological implications of bursting in mouse CCs

Whatever the ionic current components and the timing of their activation that are required to explain bursting behavior in the β2 KO cells, these results indicate that any factors that may up- or down-regulate the β2 contributions to BK channel function may produce pronounced changes in CC activity. Furthermore, the capacity of CCs to fire either spontaneous APs or spontaneous bursts suggests that other regulatory mechanisms may exist that may promote different kinds of firing patterns. This therefore prompts the following question. How might such changes between spontaneous firing versus burst firing impact CC catecholamine secretion?

One hypothesis is that down-regulation and, in particular, KO of β2 will result in reduced depolarization-evoked catecholamine secretion. However, such a proposal ignores the potential role of spontaneous, non-evoked catecholamine secretion. A previous amperometric study of secretion of catecholamines from rat CCs during different patterns of AP stimulation indicate that AP frequencies of ∼1 Hz produce little net secretion (Duan et al., 2003). In such a case, basal levels of AP firing would be unlikely to contribute appreciably to net catecholamine secretion and only depolarization-evoked secretion would play an important role in triggering catecholamine release. However, for CCs from β2 KO mice, although the overall frequency of bursts is comparable with spontaneous AP firing in native cells, the slow-wave bursts, as a consequence of a more sustained activation of Ca^{2+} channels, may result in a substantial increase in basal catecholamine release. This proposal is, in fact, supported by work comparing Ca^{2+} elevations elicited by repetitive spontaneous firing in gonadotrophs in comparison with burst firing in somatotrophs (Van Goor et al., 2001). Gonadotrophs fire spontaneously at frequencies similar to mouse CCs, but fluorescent Ca^{2+} buffers fail to report Ca^{2+} elevations in such cells. In contrast, the plateau potentials and bursts observed in somatotrophs produce robust Ca^{2+} elevation (Van Goor et al., 2001). We therefore propose that the consequences of β2 subunit KO (or down-regulation) on catecholamine secretion may be somewhat counterintuitive. Although evoked secretion perhaps activated by sympathetic nerve stimulation may be reduced as a consequence of diminished AP frequency, the present results suggest that basal CA secretion from CCs of β2 KO mice may be markedly enhanced. Future work will address this possibility.

We thank Dr. Andy Meredith for providing the *kcnma1*$^{-/-}$ mice to us. The monoclonal Ab anti-BKbeta2 (N53/32) was developed by and obtained from the University of California, Davis/National Institutes of Health (NIH) NeuroMab Facility, supported by NIH grant U24NS050606, and maintained by the Department of Neurobiology, Physiology, and Behavior, College of Biological Sciences, University of California, Davis.

This work was supported by NIH grant GM-081748 to C.J. Lingle and by grant no. P60 DK020579 to the Diabetes Research and Training Center.

The authors declare no competing financial interests.

Kenton J. Swartz served as editor.

Submitted: 30 June 2014
Accepted: 29 August 2014

REFERENCES

Contreras, G.F., K. Castillo, N. Enrique, W. Carrasquel-Ursulaez, J.P. Castillo, V. Milesi, A. Neely, O. Alvarez, G. Ferreira, C. González, and R. Latorre. 2013. A BK (Slo1) channel journey from molecule to physiology. *Channels (Austin).* 7:442–458. http://dx.doi.org/10.4161/chan.26242

Ding, J.P., Z.W. Li, and C.J. Lingle. 1998. Inactivating BK channels in rat chromaffin cells may arise from heteromultimeric assembly of distinct inactivation-competent and noninactivating subunits. *Biophys. J.* 74:268–289. http://dx.doi.org/10.1016/S0006-3495(98)77785-9

Domínguez, N., M. Rodríguez, J.D. Machado, and R. Borges. 2012. Preparation and culture of adrenal chromaffin cells. *Methods Mol. Biol.*846:223–234.http://dx.doi.org/10.1007/978-1-61779-536-7_20

Duan, K., X. Yu, C. Zhang, and Z. Zhou. 2003. Control of secretion by temporal patterns of action potentials in adrenal chromaffin cells. *J. Neurosci.* 23:11235–11243.

Faber, E.S., and P. Sah. 2003. Ca^{2+}-activated K^+ (BK) channel inactivation contributes to spike broadening during repetitive firing in the rat lateral amygdala. *J. Physiol.* 552:483–497. http://dx.doi.org/10.1113/jphysiol.2003.050120

Grimes, W.N., W. Li, A.E. Chávez, and J.S. Diamond. 2009. BK channels modulate pre- and postsynaptic signaling at reciprocal synapses in retina. *Nat. Neurosci.* 12:585–592. http://dx.doi.org/10.1038/nn.2302

Hamill, O.P., A. Marty, E. Neher, B. Sakmann, and F.J. Sigworth. 1981. Improved patch-clamp techniques for high-resolution current recording from cells and cell-free membrane patches. *Pflugers Arch.* 391:85–100. http://dx.doi.org/10.1007/BF00656997

Herrington, J., C.R. Solaro, A. Neely, and C.J. Lingle. 1995. The suppression of Ca^{2+}- and voltage-dependent outward K^+ current during mAChR activation in rat adrenal chromaffin cells. *J. Physiol.* 485:297–318.

Hicks, G.A., and N.V. Marrion. 1998. Ca^{2+}-dependent inactivation of large conductance Ca^{2+}-activated K^+ (BK) channels in rat hippocampal neurones produced by pore block from an associated particle. *J. Physiol.* 508:721–734. http://dx.doi.org/10.1111/j.1469-7793.1998.721bp.x

Horn, R., and A. Marty. 1988. Muscarinic activation of ionic currents measured by a new whole-cell recording method. *J. Gen. Physiol.* 92:145–159. http://dx.doi.org/10.1085/jgp.92.2.145

Hoshi, T., A. Pantazis, and R. Olcese. 2013. Transduction of voltage and Ca^{2+} signals by Slo1 BK channels. *Physiology (Bethesda).* 28:172–189. http://dx.doi.org/10.1152/physiol.00055.2012

Downloaded from http://rupress.org/jgp/article-pdf/144/4/275/1793887/jgp_201411253.pdf by guest on 09 February 2026

Khaliq, Z.M., and B.P. Bean. 2010. Pacemaking in dopaminergic ventral tegmental area neurons: depolarizing drive from background and voltage-dependent sodium conductances. *J. Neurosci.* 30:7401–7413. http://dx.doi.org/10.1523/JNEUROSCI.0143-10.2010

Li, W., S.B. Gao, C.X. Lv, Y. Wu, Z.H. Guo, J.P. Ding, and T. Xu. 2007. Characterization of voltage-and Ca^{2+}-activated K^+ channels in rat dorsal root ganglion neurons. *J. Cell. Physiol.* 212:348–357. http://dx.doi.org/10.1002/jcp.21007

Li, Z.W., J.P. Ding, V. Kalyanaraman, and C.J. Lingle. 1999. RINm5f cells express inactivating BK channels whereas HIT cells express noninactivating BK channels. *J. Neurophysiol.* 81:611–624.

Lingle, C.J., C.R. Solaro, M. Prakriya, and J.P. Ding. 1996. Calcium-activated potassium channels in adrenal chromaffin cells. *Ion Channels.* 4:261–301. http://dx.doi.org/10.1007/978-1-4899-1775-1_7

Lovell, P.V., D.G. James, and D.P. McCobb. 2000. Bovine versus rat adrenal chromaffin cells: big differences in BK potassium channel properties. *J. Neurophysiol.* 83:3277–3286.

Marcantoni, A., P. Baldelli, J.M. Hernandez-Guijo, V. Comunanza, V. Carabelli, and E. Carbone. 2007. L-type calcium channels in adrenal chromaffin cells: role in pace-making and secretion. *Cell Calcium.* 42:397–408. http://dx.doi.org/10.1016/j.ceca.2007.04.015

Marcantoni, A., D.H. Vandael, S. Mahapatra, V. Carabelli, M.J. Sinnegger-Brauns, J. Striessnig, and E. Carbone. 2010. Loss of Cav1.3 channels reveals the critical role of L-type and BK channel coupling in pacemaking mouse adrenal chromaffin cells. *J. Neurosci.* 30:491–504. http://dx.doi.org/10.1523/JNEUROSCI.4961-09.2010

Nassar-Gentina, V., H.B. Pollard, and E. Rojas. 1988. Electrical activity in chromaffin cells of intact mouse adrenal gland. *Am. J. Physiol.* 254:C675–C683.

Neely, A., and C.J. Lingle. 1992. Two components of calcium-activated potassium current in rat adrenal chromaffin cells. *J. Physiol.* 453:97–131.

Orio, P., Y. Torres, P. Rojas, I. Carvacho, M.L. Garcia, L. Toro, M.A. Valverde, and R. Latorre. 2006. Structural determinants for functional coupling between the β and α subunits in the Ca^{2+}-activated K^+ (BK) channel. *J. Gen. Physiol.* 127:191–204. http://dx.doi.org/10.1085/jgp.200509370

Prakriya, M., and C.J. Lingle. 2000. Activation of BK channels in rat chromaffin cells requires summation of Ca^{2+} influx from multiple Ca^{2+} channels. *J. Neurophysiol.* 84:1123–1135.

Prakriya, M., C.R. Solaro, and C.J. Lingle. 1996. $[Ca^{2+}]_i$ elevations detected by BK channels during Ca^{2+} influx and muscarine-mediated release of Ca^{2+} from intracellular stores in rat chromaffin cells. *J. Neurosci.* 16:4344–4359.

Pyott, S.J., E. Glowatzki, J.S. Trimmer, and R.W. Aldrich. 2004. Extrasynaptic localization of inactivating calcium-activated potassium channels in mouse inner hair cells. *J. Neurosci.* 24:9469–9474. http://dx.doi.org/10.1523/JNEUROSCI.3162-04.2004

Sausbier, M., H. Hu, C. Arntz, S. Feil, S. Kamm, H. Adelsberger, U. Sausbier, C.A. Sailer, R. Feil, F. Hofmann, et al. 2004. Cerebellar ataxia and Purkinje cell dysfunction caused by Ca^{2+}-activated K^+ channel deficiency. *Proc. Natl. Acad. Sci. USA.* 101:9474–9478. http://dx.doi.org/10.1073/pnas.0401702101

Shao, L.R., R. Halvorsrud, L. Borg-Graham, and J.F. Storm. 1999. The role of BK-type Ca^{2+}-dependent K^+ channels in spike broadening during repetitive firing in rat hippocampal pyramidal cells. *J. Physiol.* 521:135–146. http://dx.doi.org/10.1111/j.1469-7793.1999.00135.x

Solaro, C.R., and C.J. Lingle. 1992. Trypsin-sensitive, rapid inactivation of a calcium-activated potassium channel. *Science.* 257:1694–1698. http://dx.doi.org/10.1126/science.1529355

Solaro, C.R., M. Prakriya, J.P. Ding, and C.J. Lingle. 1995. Inactivating and noninactivating Ca^{2+}- and voltage-dependent K^+ current in rat adrenal chromaffin cells. *J. Neurosci.* 15:6110–6123.

Sun, L., Y. Xiong, X. Zeng, Y. Wu, N. Pan, C.J. Lingle, A. Qu, and J. Ding. 2009. Differential regulation of action potentials by inactivating and noninactivating BK channels in rat adrenal chromaffin cells. *Biophys. J.* 97:1832–1842. http://dx.doi.org/10.1016/j.bpj.2009.06.042

Van Goor, F., Y.X. Li, and S.S. Stojilkovic. 2001. Paradoxical role of large-conductance calcium-activated K^+ (BK) channels in controlling action potential-driven Ca^{2+} entry in anterior pituitary cells. *J. Neurosci.* 21:5902–5915.

Vandael, D.H., A. Marcantoni, S. Mahapatra, A. Caro, P. Ruth, A. Zuccotti, M. Knipper, and E. Carbone. 2010. $Ca_v1.3$ and BK channels for timing and regulating cell firing. *Mol. Neurobiol.* 42:185–198. http://dx.doi.org/10.1007/s12035-010-8151-3

Vandael, D.H., A. Zuccotti, J. Striessnig, and E. Carbone. 2012. $Ca_V1.3$-driven SK channel activation regulates pacemaking and spike frequency adaptation in mouse chromaffin cells. *J. Neurosci.* 32:16345–16359. http://dx.doi.org/10.1523/JNEUROSCI.3715-12.2012

Vandael, D.H., S. Mahapatra, C. Calorio, A. Marcantoni, and E. Carbone. 2013. Cav1.3 and Cav1.2 channels of adrenal chromaffin cells: emerging views on cAMP/cGMP-mediated phosphorylation and role in pacemaking. *Biochim. Biophys. Acta.* 1828:1608–1618. http://dx.doi.org/10.1016/j.bbamem.2012.11.013

Wallner, M., P. Meera, and L. Toro. 1999. Molecular basis of fast inactivation in voltage and Ca^{2+}-activated K^+ channels: a transmembrane β-subunit homolog. *Proc. Natl. Acad. Sci. USA.* 96:4137–4142. http://dx.doi.org/10.1073/pnas.96.7.4137

Wang, Y.-W., J.P. Ding, X.-M. Xia, and C.J. Lingle. 2002. Consequences of the stoichiometry of *Slo1* α and auxiliary β subunits on functional properties of large-conductance Ca^{2+}-activated K^+ channels. *J. Neurosci.* 22:1550–1561.

Xia, X.-M., J.P. Ding, and C.J. Lingle. 1999. Molecular basis for the inactivation of Ca^{2+}- and voltage-dependent BK channels in adrenal chromaffin cells and rat insulinoma tumor cells. *J. Neurosci.* 19:5255–5264.

Yang, C.T., X.H. Zeng, X.M. Xia, and C.J. Lingle. 2009. Interactions between β subunits of the KCNMB family and Slo3: β4 selectively modulates Slo3 expression and function. *PLoS ONE.* 4:e6135. http://dx.doi.org/10.1371/journal.pone.0006135

Yang, C., X.H. Zeng, Y. Zhou, X.M. Xia, and C.J. Lingle. 2011. LRRC52 (leucine-rich-repeat-containing protein 52), a testis-specific auxiliary subunit of the alkalization-activated Slo3 channel. *Proc. Natl. Acad. Sci. USA.* 108:19419–19424. http://dx.doi.org/10.1073/pnas.1111104108

Zeng, X.H., C. Yang, S.T. Kim, C.J. Lingle, and X.M. Xia. 2011. Deletion of the *Slo3* gene abolishes alkalization-activated K^+ current in mouse spermatozoa. *Proc. Natl. Acad. Sci. USA.* 108:5879–5884. http://dx.doi.org/10.1073/pnas.1100240108

Downloaded from http://rupress.org/jgp/article-pdf/144/4/275/1793887/jgp_201411253.pdf by guest on 09 February 2026